



Title	On the pollutant removal, dispersion, and entrainment over two-dimensional idealized street canyons
Author(s)	Liu, CH; Wong, CC
Citation	Atmospheric Research, 2014, v. 135–136, p. 128–142
Issued Date	2014
URL	http://hdl.handle.net/10722/189219
Rights	NOTICE: this is the author's version of a work that was accepted for publication in Atmospheric Research. Changes resulting from the publishing process, such as peer review, editing, corrections, structural formatting, and other quality control mechanisms may not be reflected in this document. Changes may have been made to this work since it was submitted for publication. A definitive version was subsequently published in Atmospheric Research, 2014, v. 135–136, p. 128–142. DOI: 10.1016/j.atmosres.2013.08.006

On the Pollutant Removal, Dispersion, and Entrainment over Two-Dimensional Idealized Street Canyons

Chun-Ho Liu and Colman C.C. Wong

Department of Mechanical Engineering, The University of Hong Kong, Hong Kong

Abstract

Pollutant dispersion over urban areas is not that well understood, in particular at the street canyon scale. This study is therefore conceived to examine how urban morphology modifies the pollutant removal, dispersion, and entrainment over urban areas. An idealized computational domain consisting of 12 two-dimensional (2D) identical street canyons of unity aspect ratio is employed. The large-eddy simulation (LES) is used to calculate the turbulent flows and pollutant transport in the urban boundary layer (UBL). An area source of uniform pollutant concentration is applied on the ground of the first street canyon. A close examination on the roof-level turbulence reveals patches of low-speed air masses in the streamwise flows and narrow high-speed downdrafts in the shear layer. Different from the flows over a smooth surface, the turbulence intensities are peaked near the top of the building roughness. The pollutant is rather uniformly distributed inside a street canyon but disperses quickly in the UBL over the buildings. Partitioning the vertical pollutant flux into its mean and turbulent components demystifies that the pollutant removal is mainly governed by turbulence. Whereas, mean wind carries pollutant into and out of a street canyon simul-

taneously. In addition to wind speed promotion, turbulent mixing is thus required to dilute the ground-level pollutants, which are then removed from the street canyon to the UBL. Atmospheric flows slow down rapidly after the leeward buildings, leading to updrafts carrying pollutants away from the street canyons (the basic pollutant removal mechanism).

Keywords: air quality, coherent structure, large-eddy simulation, pollutant plume dispersion, pollutant removal mechanism, urban boundary layer

1. Introduction

One of the most pronounced effects of human activities on micro-climate and air chemistry/quality is in cities (Landsberg, 1970; Minoura, 1999; Tu et al., 2007; Chang et al., 2009; Notario et al., 2012). Urban areas are the sites consisting of most anthropogenic pollutant emission (Piringer et al., 2007; Kim Oanh et al., 2008; Chen et al., 2009) where the vast majority of people live (United Nation, 2008). Yet, a greater population density could promote more efficient energy consumption and hence lower down per capita carbon footprint (Parrish and Zhu, 2009).

The scalar transport, such as heat, moisture, and pollutants, in the atmospheric boundary layer (ABL) is an attractive research topic with a range of application. Turbulent transport over a variety of natural terrain has been well explored. For example, the transport of atmospheric constituents in open, unobstructed, relatively flat and homogeneous terrain can be calculated well by the Gaussian plume model (Pasquill, 1983). On the other hand, urban morphology imposes radical changes in radiative, thermodynamic, and aerodynamic characteristics at the ABL bottom. It hence influ-

18 ences micro-climate, enhances turbulence, and modifies air pollutant mixing
19 and transport (Mazzeo and Venegas, 1991; Baklanov, 2009), giving rise to
20 the development of urban boundary layer (UBL). In the absence of any to-
21 pography, buildings are the roughness elements of a city. The major flow
22 characteristics in built areas result from building wakes, road intersections,
23 and street canyon effects. Building wakes are largely due to the flows around
24 an isolated building. Whereas, in building clusters, the wakes associated
25 with individual buildings interact with each other resulting in the recirculat-
26 ing flows at the UBL bottom. Apparently, there is a knowledge gap in urban
27 dispersion, in particular in the neighborhood scales with explicitly resolved
28 buildings in which the most serious threats to urban inhabitants, including
29 heavy vehicular exhaust and accidental toxic release, are posed.

30 Approaches to atmospheric transport in the UBL are broadly divided
31 into field measurements (Roth, 2000), laboratory experiments (Ahmad et al.,
32 2005), and mathematical modeling (Vardoulakis et al., 2003; Li et al., 2006)
33 that complement each other. Focusing on a length scale in the range 1 km
34 to 3.5 km, Britter et al. (2002) compared the accuracy of steady-state and
35 unsteady-state pollutant transport models. Rotach et al. (2005) conducted
36 the *Basel UrBan Boundary Layer Experiment* (BUBBLE) to measure tur-
37 bulence and tracer over urban, sub-urban, and rural areas. Using the same
38 UBL scenario in New York City, Hanna et al. (2006) tested five computa-
39 tional fluid dynamics (CFD) models which agreed well with the observed
40 wind flows during a field experiment. Recently, *Dispersion of Air Pollu-
41 tion and its Penetration into the Local Environment* (DAPPLE), which was
42 a major campaign focusing on the effects of city architecture and prevail-

43 ing climatic conditions in North European, was carried out in London to
44 examine the pollutant mixing and transport in a complex and dense urban
45 environment (Wood et al., 2009).

46 Although the models are necessarily simplified, a few field measurement
47 campaigns using reduced-scale building blocks have been performed to test
48 the sensitivity of UBL pollutant transport to building geometry and dimen-
49 sions. Measuring the pollutant plume dispersion from the source in the first
50 or second row over an array of cubes of size 2 m, Davidson et al. (1995) found
51 that the mean vertical plume extent increases by 40% to 50% compared with
52 that over open and flat terrain. Employing another array consisting of over
53 100 rectangular blocks of size 1.10 m \times 1.10 m \times 1.15 m (length \times width \times
54 height), Macdonald et al. (1998) investigated how the density of roughness
55 elements affects the plume dispersion behind a ground-level point source.
56 The horizontal plume coverage is about 2 to 4 times wider than that over an
57 open and flat terrain. Using a series of reduced-scale field measurements, and
58 wind tunnel and water channel experiments, Yee et al. (2006) consistently
59 found that urban obstacles modify pollutant plume dispersion substantially
60 in which the plume spread is promoted by a factor of 2 to 4.

61 To test the sensitivity of pollutant dispersion to turbulence in a con-
62 trollable manner, a number of laboratory experiments using wind tunnels
63 or water channels have been carried out to examine pollutant transport in
64 UBL. Meroney et al. (1996) implemented the technique using line sources to
65 simulate the vehicular pollutant transport in street canyons. A street canyon
66 is the basic unit constructing a city. An elucidation of its transport processes
67 can enrich the fundamental understanding of pollutant removal in entire ur-

68 ban areas. The flows over an isolated building and building clusters were
69 found to exhibit different pollutant dispersion behaviors. Afterward, the
70 spatial distributions of mean and root-mean-square (RMS) pollutant con-
71 centrations were measured by Pavageau and Schatzmann (1999) in details
72 that has been serving as a major dataset for the validation of mathematical
73 models. Earlier theoretical studies outlined the vertical profiles of (decreas-
74 ing) pollutant concentration in a street canyon. Likewise, Kastner-Klein
75 and Plate (1999) measured the pollutant concentration distributions on the
76 leeward and windward facades that are in line with the vertical profiles of de-
77 creasing pollutant concentration as found in early theoretical studies. Louka
78 et al. (2000) used field measurements to demonstrate the importance of inter-
79 mittent recirculating flows to street-level ventilation. A series of sensitivity
80 tests were performed by Chang and Meroney (2001) and Chang and Meroney
81 (2003) to study how the dimensions of buildings and streets affect pollutant
82 transport. Jiang et al. (2007) applied flow visualization in a water chan-
83 nel, illustrating the pollutant transport behaviors in step-up and step-down
84 notch street canyons. The aforementioned field measurements and labora-
85 tory experiments lay down the foundation of urban structures for atmospheric
86 dispersion in the UBL.

87 Similar to other turbulence researches, mathematical modeling has been
88 playing a major role in probing the flows and pollutant transport in urban ar-
89 eas. Using large-eddy simulation (LES), Liu and Barth (2002) and Liu et al.
90 (2005) studied the turbulent pollutant transport inside a street canyon, and
91 compared the pollutant distribution in street canyons of aspect ratio 0.5, 1,
92 and 2. Cui et al. (2004), focusing on the LES-calculated turbulence charac-

93 teristics in and over a street canyon, attempted to determine the turbulence
94 scales. Afterwards, the pollutant transport from a line source (vehicular pol-
95 lutant) or an area source (heat transfer) was examined in Cai et al. (2008).
96 Letzel et al. (2008) recently realized the functionality of Kelvin-Helmholtz
97 instabilities related to urban pollutant dispersion formulating the hypothesis
98 of the pollutant removal by turbulence rather than mean flows.

99 Although the pollutant dispersion in urban areas has been examined in
100 numerous studies, for example, the use of quadrant analysis in Cheng and
101 Liu (2011), a number of key questions remain unclear. In this paper, we
102 attempt to use LES with coherent structures to address the mechanism of
103 pollutant removal from two-dimensional (2D) idealized street canyons and
104 the pollutant transport aloft in the UBL. Moreover, a detailed analysis on
105 the turbulent flows is carried out to differentiate the role of mean wind and
106 turbulence in pollutant removal and entrainment. This section outlines the
107 problem background. The modeling details are described in Section 2. A
108 comprehensive diagnosis is conducted in Section 3. Apart from the properties
109 of flows and pollutant transport below the canopy level (Section 3.1) and in
110 the UBL over the buildings (Section 3.2), a thorough analysis on the pollutant
111 removal mechanism is performed in Section 3.3. Afterward, we look into the
112 coherent structures of flow and pollutant transport in Section 3.4 to reveal
113 their coupling. Finally, the conclusion is drawn in Section 4.

114 **2. Methodology**

115 *2.1. Governing Equations*

116 LES in the open-source CFD code OpenFOAM (2013) is used in this

117 study. The flow is assumed to be isothermal and incompressible that consists
 118 of the continuity

$$\frac{\partial \bar{u}_i}{\partial x_i} = 0 \quad (1)$$

119 and the filtered Navier-Stokes equation, written as

$$\frac{\partial \bar{u}_i}{\partial t} + \frac{\partial}{\partial x_j} \bar{u}_i \bar{u}_j = -\frac{\Delta P}{\Delta x} \delta_{i1} - \frac{\partial \bar{\pi}}{\partial x_i} - \frac{\partial \tau_{ij}}{\partial x_j} + \nu \frac{\partial^2 \bar{u}_i}{\partial x_j \partial x_j} \quad (2)$$

120 in modified form where \bar{u}_i are the resolved-scale velocity components in the
 121 i -direction, x_i the Cartesian coordinates, $\Delta P/\Delta x$ the background kinematic
 122 pressure gradient, ν the kinematic viscosity, and δ_{ij} the Kronecker delta. The
 123 resolved-scale modified pressure $\bar{\pi}$ is defined as

$$\bar{\pi} = \bar{p} + \frac{2}{3} k_{\text{SGS}} \quad (3)$$

124 where \bar{p} is the resolved-scale kinematic pressure and k_{SGS} the subgrid-scale
 125 (SGS) turbulent kinetic energy (TKE). The SGS Reynolds stresses $-\tau_{ij}$ are
 126 modeled in the form

$$-\tau_{ij} = -(\overline{u_i u_j} - \bar{u}_i \bar{u}_j) = \nu_{\text{SGS}} \left(\frac{\partial \bar{u}_i}{\partial x_j} + \frac{\partial \bar{u}_j}{\partial x_i} \right) + \frac{2}{3} k_{\text{SGS}} \delta_{ij} \quad (4)$$

127 using the Smagorinsky SGS model (Smagorinsky, 1963). Here, ν_{SGS} ($=$
 128 $C_k k_{\text{SGS}}^{1/2} \Delta$) is the kinematic eddy viscosity, Δ ($= [\Delta_1 \Delta_2 \Delta_3]^{1/3}$) the filter width,
 129 and C_k ($= 0.07$) the empirical modeling constant. The one-equation SGS
 130 model (Schumann, 1975)

$$\frac{\partial k_{\text{SGS}}}{\partial t} + \frac{\partial}{\partial x_i} k_{\text{SGS}} \bar{u}_i = -\frac{1}{2} \tau_{ij} \frac{\partial \bar{u}_i}{\partial x_j} + (\nu + \nu_{\text{SGS}}) \frac{\partial^2 k_{\text{SGS}}}{\partial x_i \partial x_i} - C_\epsilon \frac{k_{\text{SGS}}^{3/2}}{\Delta} \quad (5)$$

131 is used to solve the SGS TKE conservation where C_ϵ ($= 1.05$) is another
 132 empirical modeling constant. This approach has been used in our previous
 133 studies of flows and pollutant transport over street canyons.

134 The pollutant transport is calculated by the advection-diffusion equation
 135 of a passive and inert scalar

$$\frac{\partial \bar{\phi}}{\partial t} + \frac{\partial}{\partial x_i} \bar{\phi} \bar{u}_i = -\frac{\partial \gamma_i}{\partial x_i} + \frac{\nu}{Sc} \frac{\partial^2 \bar{\phi}}{\partial x_i \partial x_i} \quad (6)$$

136 where $\bar{\phi}$ is the resolved-scale pollutant concentration and Sc ($= 0.72$) the
 137 Schmidt number. The SGS pollutant flux is modeled in the form

$$\gamma_i = \overline{\phi u_i} - \bar{\phi} \bar{u}_i = -\frac{\nu_{SGS}}{Sc} \frac{\partial \bar{\phi}}{\partial x_i}. \quad (7)$$

138 2.2. Computational Domain and Boundary Conditions

139 Different from some previous studies using cubes (Coceal et al., 2006;
 140 Kanda, 2006), the current LES computational domain (Fig. 1) is homoge-
 141 neous in the spanwise direction that consists of 12 identical, idealized street
 142 canyons of height h at the bottom and the UBL of depth H ($= 7h$) above
 143 the buildings. The buildings measure d ($= h$) in length and $5h$ in width that
 144 are evenly placed at a separation b ($= h$) apart constructing street canyons
 145 of unity aspect ratio in this study.

146 The flow is driven by the background kinematic pressure gradient $\Delta P / \Delta x$
 147 in the UBL only that results in the prevailing wind speed U at the domain top
 148 $z = H$. The prevailing wind, whose direction is aligned by δ_{i1} in Equation (2),
 149 is perpendicular to the street axis representing the worst scenario of urban
 150 pollutant removal. The boundary conditions (BCs) of the flow are periodic
 151 in the streamwise and spanwise directions. No-slip BCs, using a wall model
 152 (Spalding, 1962), are prescribed on all rigid walls. The implementation of
 153 wall model for flows over street canyons was detailed in Cheng and Liu (2011).
 154 Its major function is to ensure that the near-wall shear force is well balanced

155 even if the surface sublayer is not resolved to fine resolution. A shear-free
156 boundary is applied at the domain top. The aforementioned configuration
157 represents fully developed turbulent flow in an open channel with a rough
158 bottom surface.

159 The ground of the first street canyon right after the inflow boundary is a
160 surface of constant concentration Φ serving the area pollutant source in the
161 LES by the Dirichlet BC $\bar{\phi} = \Phi$. The use of a constant-concentration BC also
162 facilitates the interpretation of energy transport from a surface of constant
163 temperature because of the analogy between heat and mass transfer. At the
164 inflow, the concentration is zero so no background pollutant is considered.
165 At the outflow, an open boundary for pollutant

$$\frac{\partial \bar{\phi}}{\partial t} + \bar{u} \frac{\partial \bar{\phi}}{\partial x} = 0 \quad (8)$$

166 is assumed hence the pollutant is carried away from the computational do-
167 main by the prevailing flow. Zero-gradient BCs of pollutant are applied along
168 the domain top and the solid boundaries.

169 *2.3. Numerical Methods*

170 In the current LES, the implicit second-order accurate backward differ-
171 encing is used in the temporal domain. The second-order accurate Gaussian
172 finite volume integration scheme, which is based on the summation on cell
173 faces, is adopted in the calculation of gradient, divergence, and Laplacian
174 terms. The values on cell faces are interpolated by the central differencing of
175 the values at centers. The gradient normal to a surface (used in the Lapla-
176 cian terms) is calculated by the explicit non-orthogonal correction method.

177 $32 \times 160 \times 32$ (streamwise \times spanwise \times vertical) and $768 \times 160 \times 280$ ele-
 178 ments were discretized, respectively, in each street canyon and the UBL such
 179 that the total number of elements exceeds 34 million. The first element is
 180 placed at $z^+ \approx 5$ away from the nearby solid boundary so that the spatial
 181 resolution is reasonably fine enough handling the near-wall flows. The LES is
 182 integrated for over 1,600 time steps and the time increment Δt is $0.015h/U$.
 183 The Reynolds number based on the free-stream speed and the building height
 184 $Re (= Uh/\nu)$ is 10,000 and the Reynolds number based on friction velocity
 185 $Re_\tau (= u_\tau h/\nu)$ is 837. The friction velocity $u_\tau (= [\tau_w/\rho]^{1/2}$ where τ_w is the
 186 shear stress over the street canyons and ρ the fluid density) is calculated by
 187 the force balance in the streamwise direction $u_\tau = (\Delta P/\Delta x \times H)^{1/2}$. The
 188 shear stress profile is linear in the vertical direction. The numerical method-
 189 ology is detailed elsewhere (Wong and Liu, 2010a,b).

190 **3. Results and Discussion**

191 In this paper, we focus on both below the canopy level and over the street
 192 canyons. The flows and pollutant transport are examined that are discussed
 193 in this section.

194 *3.1. Below the Roof Level*

195 *3.1.1. Flow Field*

196 Fig. 2 shows the vertical profiles of the ensemble average streamwise ve-
 197 locity $\langle \bar{u} \rangle$ on the 5 vertical planes of a street canyon ($x = 0$ is the street
 198 center). Because the flows are cyclic in the streamwise direction, ensemble
 199 averaging is applied on the 12 identical street canyons which is represented

200 by angular parentheses $\langle \bar{\psi} \rangle$. The characteristic velocity scale U_s is the mean
 201 wind speed in the UBL within $h \leq z \leq 1.5h$. A noticeable velocity gradient
 202 is developed along the roof level. It is steep on the leeward side (downwind
 203 side after a building) because of the flow separation at the leeward building
 204 edge. The gentle velocity gradient on the windward side (upwind side before
 205 a building) partly signifies the thorough turbulent mixing which entrains mo-
 206 mentum into the street canyon. For a street canyon of unity aspect ratio in
 207 the skimming flow regime (Oke, 1988), the flow inside is shear driven moving
 208 toward the windward side in the upper part. The average wind speed in the
 209 street is about 10% of U_s , representing the rather weak downward momentum
 210 transport to the ground level.

211 Fig. 3 compares the vertical profiles of the ensemble average vertical veloc-
 212 ity $\langle \bar{w} \rangle$. The upward flow on the leeward side carries aged air away from the
 213 street canyon. On the windward side, the downward flow entrains relatively
 214 cleaner air aloft to make up the aged air. Combining with the characteristic
 215 streamwise flow (Fig. 2), a clockwise recirculation occupying the entire street
 216 canyon is clearly depicted whose rotation speed is no more than $0.5U_s$.

217 Fig. 4 shows the vertical profiles of the ensemble average resolved-scale
 218 TKE ($= \langle u''u'' + v''v'' + w''w'' \rangle / 2$) in and over the street canyons. Here, dou-
 219 ble prime denotes the deviation of the variable from its ensemble average ψ''
 220 ($= \bar{\psi} - \langle \bar{\psi} \rangle$) and TKE_s is the mean resolved-scale TKE in the UBL within
 221 $h \leq z \leq 1.5h$. The large $\langle \text{TKE} \rangle$ over the street canyon is attributed to
 222 the shear layer. On the contrary, the small and rather uniformly distributed
 223 $\langle \text{TKE} \rangle$ inside the street canyon (10% to 20% of TKE_s) is caused by the weak
 224 recirculating flows below the roof level. Wind shear is the only mechani-

225 cal turbulence production in isothermal flows, the strong velocity gradient
 226 originated from the flow separation at the leeward building edge is hence
 227 the major source. The TKE is peaked on the windward roof level instead
 228 of coinciding with the maximum wind shear, suggesting the importance of
 229 advection redistributing TKE inside the street canyon. Vertical mixing con-
 230 tinues as the flow moves from the leeward to windward sides and is reflected
 231 in the more gentle windward TKE gradient.

232 The coefficient of skewness

$$s_\psi = \langle \psi''^3 \rangle / \langle \psi'' \psi'' \rangle^{3/2} \quad (9)$$

233 and the coefficient of kurtosis

$$k_\psi = \langle \psi''^4 \rangle / \langle \psi'' \psi'' \rangle^2 \quad (10)$$

234 are commonly used to measure, respectively, the degree of asymmetry and
 235 peakedness of turbulence signals. Coefficient of skewness measures the di-
 236 rection and degree of asymmetry of the probability density function (PDF).
 237 It equals 0 for a symmetric (normal) distribution. Positive values for the
 238 coefficient of skewness indicate a distribution that is weighted towards the
 239 positive direction and vice versa. Coefficient of kurtosis measures the degree
 240 of peaking or flatness of a distribution. It equals 3 for a normal distribution
 241 so the excess kurtosis ($= k_\psi - 3$) is often used instead. A positive value of
 242 the excess kurtosis indicates a peaked distribution compared with the normal
 243 distribution while negative a flat one.

244 The PDF of the streamwise turbulent velocity is symmetrical except near
 245 roof level where it becomes skewed in the shear layer, as is evidenced by the
 246 sharp-peak in s_u (Fig. 5). The positive s_u also signifies that the characteristic

247 flow structures are comprised of patches of low-speed air mass and narrow
248 high-speed air masses along the roof level. This finding is in line with the
249 low-momentum fluid close to the plane of building roof observed in Michioka
250 et al. (2011b). A narrow region of large s_u is located in the area $-0.25 \leq$
251 $x/h \leq 0$, near roof level. The region spreads and descends somewhat in
252 moving toward $x/h = 0.4$ whilst the peak value significantly decreases. The
253 PDF thus tends to return to a normal distribution most likely because of the
254 enhanced turbulent mixing following the clockwise-rotating recirculation.

255 Similar to its skewness counterpart, the kurtosis of the streamwise velocity
256 k_u is peaked in $-0.25 \leq x/h \leq 0$ (Fig. 6). Hence, the patches of slow
257 streamwise-moving air masses are most likely to be found on the leeward
258 side. The profile of kurtosis of the streamwise velocity spreads out while
259 moving toward the windward side, signifying the return to a flat PDF close
260 to the normal distribution. The large positive kurtosis also shows that slow-
261 moving air masses are more common on the leeward side.

262 Analogously, the skewness of the vertical velocity s_w deviates from that
263 of the normal distribution substantially along the roof level (Fig. 7). Owing
264 to the strong shear, the broad peak of s_w is negative, located just below the
265 roof level, illustrating the dominance of roof-level updrafts and a few nar-
266 row high-speed downdrafts. The roof-level ensemble average vertical speed
267 is close to zero because of the isolated recirculation in the skimming flow
268 regime. The narrow downdrafts then govern the turbulence entrainment into
269 the street canyons. Although the shear is weak near the windward wall, s_w
270 weights toward the negative direction in which the narrow downdrafts pen-
271 etrate all the way down to the ground level. These large-scale, persistent

272 downdrafts are likely caused by the vigorous wall jet carrying fresh air en-
273 trainment and turbulence along the windward facade. Similarly, s_w leaned
274 toward the positive direction near the leeward facade in which the narrow
275 updrafts are initiated by the upward flows of the clockwise recirculation.

276 A mild peak of kurtosis of the vertical velocity k_w is found right below the
277 roof level (Fig. 8). Similar to other statistic properties, the k_w peak descends
278 in the streamwise direction following the primary clockwise recirculation. It
279 is noteworthy that a broad peak of positive excess kurtosis is observed on
280 the windward side at $x = 0.4b$. Hence, the strongest, narrow downdrafts are
281 concentrated in the vicinity to the windward facade entraining turbulence
282 and fresh air along with the wall jet down to the ground level.

283 Also shown in Figs. 2 to 8 are the wind tunnel measurements (Brown
284 et al., 2000) and the LES results (Cui et al., 2004) available in literature.
285 The profiles of streamwise (Fig. 2) and vertical (Fig. 3) velocity obtained
286 from different studies agree well with each other. Whereas, the rotating
287 speed of the (clockwise) recirculation in the street canyon obtained in Brown
288 et al. (2000) is higher than that of Cui et al. (2004) and the current LES.
289 Besides, the wind-tunnel measured TKE is higher than that of the two LESs.
290 Turbulence is purposely produced by vortex generators to model the ABL
291 in the wind tunnel. On the contrary, the LES turbulence is only generated
292 mechanically by wind shear and Reynolds stresses. The flows and turbulence
293 in the wind tunnel experiment are likely stronger than its LES counterparts.

294 The velocity skewness (Figs. 5 and 7) and kurtosis (Figs. 6 and 8) are also
295 comparable with each other. In particular, the roof-level skewed flows are
296 consistently revealed by the wind tunnel experiments and LESs. However,

297 the skewness s_w and kurtosis k_w of the vertical velocity on the windward side
298 show a little discrepancy among different studies that is likely caused by the
299 abrupt entrainment from the prevailing flow.

300 While most studies have focused on the turbulence statistics inside or
301 close to street canyons, we compare the current LES with our previous one
302 (Cheng and Liu, 2011) in which a smaller spatial domain ($H = 6h$ and three
303 street canyons) was used to contrast the different UBL flow characteristics.
304 As shown in Fig. 2, the ensemble average streamwise velocity calculated by
305 the current LES is smaller than that reported in Cheng and Liu (2011). It
306 could be a result of the shallower UBL (shorter vertical domain extent) or
307 the flow was not fully developed in our previous study so the prevailing winds
308 right over the buildings are accelerated. On the other hand, the ensemble
309 average vertical velocity calculated by both LESs is almost zero due to the
310 horizontal homogeneity (Fig. 3). Nevertheless, the differences in mean flows
311 are small compared with those in turbulence statistics.

312 The TKE calculated by the two LESs is at the same level in the vicinity
313 to the roof level, however, the value calculated by Cheng and Liu (2011)
314 decreases sharply in the UBL core (Fig. 4). Apparently, this difference in
315 TKE is a result of the no-slip top BCs adopted such that the TKE tends to
316 diminish toward the upper domain boundary. In case the UBL is too shallow
317 or remains developing, the constant shear layer is too thin that would under-
318 estimate the vertical transport right over the buildings. The uncertainties in
319 TKE subsequently affect the skewness and kurtosis of velocity components.
320 The streamwise (Fig. 5) and vertical (Fig. 7) velocities show, respectively,
321 negative skewed and positive skewed peaks in the UBL at $z = 4h$. Whilst,

322 the turbulence statistics should resume to normal distribution in the vertical
 323 direction because of the reducing shear stress in the UBL core. We believe
 324 that this discrepancy is caused by the diminishing TKE in the shallow UBL,
 325 over amplifying the skewness calculated by Cheng and Liu (2011). The above
 326 explanation also applies to the peaks of kurtosis above roof level calculated
 327 in our previous LES (Figs. 6 and 8).

328 *3.2. Over the Roof Level*

329 In the UBL over the buildings, the street canyons are treated as homo-
 330 geneous urban roughness elements so the ensemble average flow properties
 331 $\langle \psi_{\text{flow}} \rangle$ are taken in both the streamwise x and spanwise y directions. On the
 332 other hand, the pollutant source is only assigned on the ground in the first
 333 street canyon, the ensemble average pollutant properties $\langle \psi_{\text{pollutant}} \rangle$ are taken
 334 in the spanwise direction only that are reported on the vertical x - z plane.

335 *3.2.1. Flow Field*

336 A sensitivity test is performed to examine how the domain size affects the
 337 flows and the length scale of the eddies. The autocorrelation (Pope, 2009)

$$R_{\psi\psi}(x_0, \delta x) = \frac{\langle \psi''(x_0) \psi''(x_0 + \delta x) \rangle}{\langle \psi''(x_0) \psi''(x_0) \rangle} \quad (11)$$

338 of the velocity components in the streamwise direction are depicted in Fig. 9.
 339 The decreasing trends of autocorrelation of the spanwise R_{vv} and the vertical
 340 R_{ww} velocities exhibit a similar pattern that diminishes rapidly within the
 341 current LES streamwise domain extent. However, the autocorrelation of the
 342 streamwise velocity R_{uu} persists unless the elevation z is lower than $1.7h$.
 343 This finding is in line with our presumption that eddy size increases at a

344 higher elevation. The faster decreasing $R_{\psi\psi}$ near the roof level is a result of
 345 the eddy size related to urban roughness. The size of the roof-level eddies is
 346 limited by the street width that is obviously smaller than that in the UBL
 347 and so is the integral length scale. Although the current LES domain size is
 348 larger than that of the direct numerical simulation (DNS) over an array of
 349 staggered cubes by Coceal et al. (2006) by 50%, the LES-calculated R_{uu} still
 350 persists around 0.1 that is only slightly lower than its DNS counterpart. The
 351 different building geometries in the DNS and the LES could be the major
 352 reason. The autocorrelation shows that the current LES domain is just large
 353 enough for the largest eddies. While our major concern is the near-roof
 354 region, it is adopted in this study.

355 Fig. 10 compares the profile of the current LES-calculated mean stream-
 356 wise velocity $\langle \bar{u} \rangle$ with those of analytical solution and other numerical models
 357 in the UBL. It is observed that the LES is close to the 1/4 power law and
 358 the log law ($u^+ = 1/\kappa \times \ln z^+ + 5.5$) instead of the analytical 1/7 power law
 359 for flows over smooth surface (Douglas et al., 1995). The profile of Coceal
 360 et al. (2006) is slightly higher in the domain core, in which the difference
 361 is likely caused by the enhanced turbulent mixing in and over the staggered
 362 cubes. Cheng and Liu (2011) and the current study have used the same
 363 CFD LES code, whereas, the former shows a more uniform speed at the
 364 mid level of the domain in $0.2H \leq (z - h) \leq 0.8H$. The dissimilar domain
 365 size could be the major reason. Only 3 street canyons were used in Cheng
 366 and Liu (2011) while a much longer streamwise extent consisting of 12 street
 367 canyons are used in the current LES. The larger domain size can accommo-
 368 date more large, energy-carrying eddies in the UBL that avoids development

369 of effectively infinitely long eddies overpredicting the turbulent mixing.

370 The vertical profiles of RMS velocity $\langle u''_i u''_i \rangle^{1/2}$, which is the major driv-
371 ing force for turbulent mixing and transport, are illustrated in Fig. 11. Once
372 2D street canyons are introduced to the UBL bottom, the maximum RMS
373 streamwise velocity $\langle u'' u'' \rangle^{1/2}$ shifts downward to the roof level because of
374 the form drag, sharp velocity gradient, and locally elevated turbulence pro-
375 duction. The streamwise RMS velocity $\langle u'' u'' \rangle^{1/2}$ decreases with increasing
376 height that is a result of the gentler velocity gradient in the UBL core. The
377 maximum spanwise RMS velocity $\langle v'' v'' \rangle^{1/2}$ elevates a little over the roof
378 level. Finally, the vertical RMS velocity $\langle w'' w'' \rangle^{1/2}$ is peaked at $0.25h$ over
379 the roof level similar to that in Cheng and Liu (2011).

380 Also shown in Fig. 11 are the vertical profiles of RMS velocities in the
381 turbulent boundary layer over various solid boundaries. Nagaosa (1999) con-
382 sidered the flows over a smooth surface at a Reynolds number, based on the
383 channel depth, $Re = 2,300$ ($Re_\tau = 150$) using DNS. The maximum $\langle u''_i u''_i \rangle^{1/2}$
384 is located away from the wall that is in line with the characteristic in a
385 turbulent boundary layer (Kim et al., 1987). Also using DNS, Ashrafian
386 et al. (2004) studied the flows over 2D ribs of aspect ratio $1/8$ in the isolated
387 roughness regime. The maximum RMS horizontal velocities are located at
388 the roof level, while the maximum RMS vertical velocity is located at $z =$
389 $1.15h$ that is higher than that of the current LES. Coceal et al. (2006) exam-
390 ined the flows over an array of staggered cubes using DNS. The maximum
391 RMS streamwise velocity is also located at the roof level but the magnitude
392 is slightly higher than that of the current LES over 2D street canyons.

393 *3.2.2. Pollutant Transport*

394 Fig. 12 depicts the ensemble average pollutant concentration $\langle \overline{\phi} \rangle$ on the
395 vertical x - z plane. The UBL pollutant distribution generally resembles the
396 Gaussian plume shape (Wong and Liu, 2010a,b). Except in the first street
397 canyon with the ground-level pollutant source, the pollutant is quite well
398 mixed and no noticeable variation of pollutant distribution is observed in
399 the street canyons. A close examination on the tracer shows that the pol-
400 lutant concentration decays in the vertical and likewise in the longitudinal
401 direction having reached a local maximum (Fig. 13). Right at the roof level,
402 the decreasing pollutant concentration exhibits different patterns over the
403 building roofs and the street canyons. It is more uniform over the building
404 roofs but is decreased more rapidly over the street canyons. This different
405 pollutant dispersion behavior is mainly due to the enhanced pollutant mix-
406 ing over the street canyons compared with that over buildings. Besides, the
407 pollutant concentration gradient is steeper on the leeward side (than that on
408 the windward side). It is a result of the clockwise recirculation which car-
409 ries polluted air masses upward out of the street canyons along the leeward
410 building facades.

411 Fig. 14 depicts the contours of RMS pollutant concentration $\langle \phi'' \phi'' \rangle^{1/2} / \Phi$.
412 Two peaks of RMS pollutant concentration are observed in the first street
413 canyon with pollutant source. The broad maximum ground-level $\langle \phi'' \phi'' \rangle^{1/2}$
414 is mainly due to the sharply elevated pollutant concentration right over the
415 pollutant source. That it extends to the leeward side is a result of the primary
416 clockwise recirculation in a street canyon in skimming flow. Another peak
417 $\langle \phi'' \phi'' \rangle^{1/2}$ resides at the roof level. Because turbulence is the sole driving force

418 for the pollutant mixing in isothermal conditions, the roof-level peak RMS
419 pollutant concentration is attributed to the locally elevated concentration
420 gradient. This roof-level maximum $\langle \phi'' \phi'' \rangle^{1/2}$ also signifies the importance of
421 turbulence in the pollutant removal from a street canyon. It is noteworthy
422 that the peak $\langle \phi'' \phi'' \rangle^{1/2}$ does not exactly coincide with the maximum wind
423 shear on the leeward side but is shifted to the windward side, suggesting
424 the importance of advection redistributing TKE from the leeward to the
425 windward sides in a street canyon.

426 In the absence of pollutant source from the street canyon, the RMS pol-
427 lutant concentration in the second street canyon is much smaller than that
428 in the first. The broad peak of $\langle \phi'' \phi'' \rangle^{1/2}$ is on the windward side following
429 the entrainment into the street canyon. The RMS pollutant concentration
430 is unnoticeable in the rest of the street canyons, implying that the pollutant
431 concentration is rather steady and uniform in the street canyons without any
432 ground-level pollutant source.

433 *3.3. Pollutant Removal Mechanism*

434 A few studies have been performed to elucidate the pollutant removal
435 mechanism from 2D street canyons. Lee and Park (1994) and Sini et al.
436 (1996) used the exponential decay time constant and the integral dilution
437 time scale to measure pollutant removal rate. Using wind tunnel mea-
438 surements, the convective pollutant transfer velocity/coefficient have been
439 proposed by Barlow and Belcher (2002) and Narita (2007) to compare the
440 pollutant removal efficiency from street canyons of different aspect ratios.
441 Likewise, Bentham and Britter (2003) and Bady et al. (2008) employed an-
442 alytical solutions to derive pollutant exchange velocity, purging flow rate,

443 visitation frequency (number of times of a pollutant particle enters the con-
444 trol volume and passes through it), and residence time. Using LES, Liu et al.
445 (2005) modified the concept of air exchange rate (ACH) in building services
446 engineering formulating the pollutant exchange rate (PCH) to examine the
447 pollutant removal from a 2D street canyon. The PCH of an idealized 2D
448 street canyon flanked by buildings of equal height is defined as

$$\text{PCH}(t) = \int_{\Gamma} [\bar{w}(t) \bar{\phi}(t)]_{\text{roof}} d\Gamma \quad (12)$$

449 where the subscript *roof* signifies that the properties are normal to the roof
450 of the street canyon Γ . In view of the direction of the vertical velocity \bar{w} ,
451 positive PCH represents pollutant removal while negative PCH pollutant
452 entrainment. Decomposing PCH into the mean and turbulent components,
453 and taking ensemble average yields

$$\begin{aligned} \langle \text{PCH}(t) \rangle &= \langle \text{PCH} \rangle \\ &= \langle \overline{\text{PCH}} \rangle + \langle \text{PCH}'' \rangle \\ &= \int_{\Gamma} [\langle \bar{\phi} \rangle \langle \bar{w} \rangle + \langle \phi'' w'' \rangle]_{\text{roof}} d\Gamma \end{aligned} \quad (13)$$

454 that measures the relative contributions from the mean $\langle \bar{\phi} \rangle \langle \bar{w} \rangle$ and turbulent
455 $\langle \phi'' w'' \rangle$ pollutant fluxes to the total pollutant removal. Therefore, PCH has
456 two parts, as defined in the integral Equation (13), one due to the mean
457 values and the other the mean of the correlation between flows and pollutant
458 concentration. In the current LES, $\langle \overline{\text{PCH}} \rangle$ is negative (less than 10% of
459 $\langle \text{PCH} \rangle$) in the first street canyon with pollutant source, signifying pollutant
460 entrainment by mean flow. As such, the turbulent component $\langle \text{PCH}'' \rangle$ is
461 responsible carrying pollutant away from the street canyon.

462 Fig. 15 depicts the ensemble average mean pollutant flux $\langle \bar{\phi} \rangle \langle \bar{w} \rangle / \Phi / U$
 463 turbulent pollutant flux $\langle \phi'' w'' \rangle / \Phi / U$ and total pollutant flux $(\langle \bar{\phi} \rangle \langle \bar{w} \rangle + \langle \phi'' w'' \rangle) / \Phi / U$
 464 along the roof level of the street canyons. Please note that only the first street
 465 canyon is installed with pollutant source. The ensemble average mean pollu-
 466 tant flux is decreased in the streamwise direction (Fig. 15a) that is attributed
 467 to the inhomogeneous ground-level pollutant source and the exponentially
 468 decaying pollutant concentration. The pollutant is removed ($\langle \bar{\phi} \rangle \langle \bar{w} \rangle / \Phi / U$
 469 > 0) and is entrained ($\langle \bar{\phi} \rangle \langle \bar{w} \rangle / \Phi / U < 0$) on the leeward and wind-
 470 ward side, respectively, following the primary clockwise recirculation in the
 471 street canyons. As shown by the sharp roof-level $\langle \bar{\phi} \rangle \langle \bar{w} \rangle / \Phi / U$, the pollu-
 472 tant is removed abruptly right at the roof-level windward edge because of the
 473 flow impingement. Fig. 15b shows that the turbulent pollutant flux largely
 474 accounts for the pollutant removal. Only a tiny negative $\langle \phi'' w'' \rangle / \Phi / U$ is
 475 observed close to the roof-level leeward building edge, thus, its contribution
 476 to the overall pollutant entrainment is insignificant. Moreover, the turbulent
 477 pollutant flux is comparable to its mean counterpart only in the first street
 478 canyon with the pollutant source. In the rest of the street canyons, the tur-
 479 bulent pollutant flux is negligible, clarifying the different roles of mean and
 480 turbulent components in the total pollutant removal. We thus hypothesize
 481 that the pollutant removal mechanism in 2D street canyons is mainly gov-
 482 erned by turbulent mixing, dilution, then advection out of the street canyon
 483 to the UBL to reduce the ground-level pollutant concentration.

484 Combining the mean and turbulent pollutant fluxes yields the total pol-
 485 lutant flux $(\langle \bar{\phi} \rangle \langle \bar{w} \rangle + \langle \phi'' w'' \rangle) / \Phi / U$ (Fig. 15c). In the first street canyon,
 486 the net pollutant removal is positive that offsets the pollutant emission at the

487 ground level. Moreover, $\langle \overline{\text{PCH}} \rangle$ and $\langle \text{PCH}'' \rangle$ are comparable to each other.
488 In the rest of the street canyons without pollutant source, $\langle \text{PCH}'' \rangle$ is smaller
489 than $\langle \overline{\text{PCH}} \rangle$ by an order of magnitude so the net $\langle \overline{\text{PCH}} \rangle$ equals zero that
490 carries pollutant into and out of the street canyons simultaneously.

491 *3.4. Coherent Structures*

492 Ensemble average quantities are used in the previous sections studying
493 the turbulent transport in 2D street canyons. Additional perspective about
494 the turbulent transport processes, especially the pollutant removal mecha-
495 nism, could be accomplished by looking into the coherent structures of the
496 instantaneous flow variables. These data are snapshots of the LES that are
497 considered typical structures of flows and pollutant transport.

498 Fig. 16 compares the instantaneous vertical momentum flux $u''w''$ at dif-
499 ferent levels over and inside the street canyons. At $z = 2h$ in the UBL core,
500 the flow is dominated by the coherent structures of negative vertical momen-
501 tum flux, suggesting that most of the fast-moving (slow-moving) streamwise
502 flowing air masses are downward (upward) moving (Fig. 16a). This negative
503 correlation between the streamwise and vertical flows in turn signifies the
504 majority momentum transport from the prevailing flow down to the lower
505 UBL entraining into the street canyons. At a lower elevation $z = 1.2h$ close to
506 the roof level (Fig. 16b), the vertical momentum flux is also mostly negative.
507 Different from that in the UBL core, its structures are mildly elongated in the
508 streamwise direction. Whereas, no alternative high- and low-speed elongated
509 structures are clearly found yet. In the region very close to the roof level at z
510 $= 1.05h$ (Fig. 16c), the elongated flow structures no longer exist that are re-
511 placed by patches of negative vertical momentum flux over the street canyons.

512 These downward moving coherent structures, which are partly attributed to
513 the form drag of the buildings, transfer momentum into the street canyons
514 through the shear layer at roof level. As shown in Fig. 16d, the negatively
515 correlated roof-level streamwise and vertical velocities are consistent with the
516 positive skewed streamwise velocity (Fig. 5) and the negative skewed vertical
517 velocity (Fig. 7) along the roof level (Section 3.1.1). Momentum entrains
518 down into the street canyon to drive the primary recirculation, the vertical
519 momentum flux at the street-canyon mid level ($z = 0.5h$) is therefore positive
520 (Fig. 16e), suggesting the advection dominated momentum transport.

521 Fig. 17 illustrates the LES-calculated snapshots of streamwise slow-moving
522 (Fig. 17a) and fast-moving (Fig. 17b) air masses. Similar to the flows in other
523 studies available in literature, sparse air masses carrying negative momentum
524 fluxes are found in the UBL demonstrating the downward momentum trans-
525 fer from the prevailing flow. Slow-moving air masses, which are partly due
526 to the drag of the buildings, are consistently observed at the roof level of the
527 street canyons (Fig. 17a). These coherent structures are also dominated by
528 the updrafts of positive fluctuating vertical velocity w'' , that in turn suggests
529 the characteristic vertical momentum transfer. These downward vertical mo-
530 mentum fluxes are also revealed in Fig. 16 and in wind tunnel experiments
531 in the form of sweeps and ejections (Michioka et al., 2011a).

532 Fig. 18 switches the contours of vertical fluctuating velocity w'' to the
533 fluctuating pollutant concentration ϕ'' on the patches of air masses. Along
534 the roof level, the fluctuating pollutant concentration is negative on those
535 slow-moving air masses (Fig. 18a). Hence, polluted air masses slow down
536 ($u'' < 0$) and move upward ($w'' > 0$) leading to the decreasing instantaneous

537 pollutant concentration ($\phi'' < 0$) over the street canyons. This momentum
538 transfer, from the horizontal to the vertical, formulates the basic mechanism
539 of pollutant removal from a street canyon in skimming flow. In the UBL
540 aloft, fast-moving air masses lower down their pollutant concentration due
541 to streamwise advection (Fig. 18b). It is noteworthy that the aforementioned
542 upward-moving coherent structure was also revealed in the particle
543 image velocimetry (PIV) experiments by Takimoto et al. (2011). They used
544 the term flushing to represent this upward air movement across the entire
545 street canyon. Recently, Michioka and Sato (2012), using different incoming
546 turbulent flow structures, showed that the pollutant removal is attributed to
547 the low-momentum fluid. The amount of pollutant removal is closely related
548 to the size of the coherent structure.

549 As discussed mathematically in Section 3.3, the fluctuating vertical ve-
550 locity w'' accounts for the pollutant removal from the street canyons to the
551 UBL. Snapshots of downdrafts ($w'' < 0$) and updrafts ($w'' > 0$) are depicted
552 in Figs. 19a and 19b, respectively. Large downdrafts with negative pollutant
553 concentration fluctuation are identified at around $z = 2h$ (Fig. 19a), suggest-
554 ing the downward fresh air entrainment for pollutant dilution. Updrafts are
555 shown in Fig. 19b with positive fluctuating pollutant concentration. These
556 uprising air masses carry pollutants from the street canyons to the roof level
557 and finally to the UBL aloft governing the basic pollutant removal.

558 **4. Conclusions**

559 In view of the rapid urbanization and heavy vehicular pollutant emission,
560 a numerical analysis using LES is carried out to advance our basic under-

561 standing of pollutant removal from urban street canyons. Decomposing the
562 roof-level vertical pollutant flux into its mean and turbulent components
563 reveals that pollutant removal from a street canyon is dominated by tur-
564 bulence. Turbulent mixing dilutes the ground-level pollutant which is then
565 purged away by the prevailing flow. On the other hand, mean wind drives
566 pollutant into and out of a street canyon simultaneously, ending up with
567 insignificant net pollutant exchange. A detailed investigation of the statistic
568 properties and coherent structures of the turbulence in the UBL unveils that
569 the streamwise flows decelerate (accelerate) over the street canyons (build-
570 ings). The slow-moving flows are results of momentum entrainment into the
571 street canyons driving the recirculating flows. Besides, the negative fluctuat-
572 ing streamwise velocity gives rise to the upward moving air masses carrying
573 the pollutant out of a street canyon. These findings collectively formulate
574 the basic turbulent pollutant removal mechanisms in urban street canyons
575 in the skimming flow regimes. The results also shade some light on the
576 functionality of turbulence over urban areas from the air quality perspective
577 and arouse the benefit of promoting both mean winds and turbulence for
578 pollutant removal from street level in dense compact cities.

579 *Acknowledgments*

580 This study was jointly supported by the Strategic Research Areas and
581 Themes, *Computational Sciences*, and the University Research Committee
582 *Seed Funding Programme of Basic Research* 200910159028, 201011159166,
583 and 201111159166 of the University of Hong Kong. The computation is
584 supported in part by a Hong Kong UGC Special Equipment Grant (SEG

585 HKU09). The technical support from Lilian Y.L. Chan, Frankie F.T. Che-
586 ung, Tony W.K. Cheung, W.K. Kwan, and N.S. Mok with HKU ITS is
587 appreciated. Last but not least, we deeply thank the anonymous reviewers
588 for their constructive reviews and insightful comments.

589 **References**

590 Ahmad, K., Khare, M., Chaudhry, K. K., 2005. Wind tunnel simulation
591 studies on dispersion at urban street canyons and intersections - a review.
592 *J. Wind Engg. & Ind. Aerodyn.* 93, 697–717.

593 Ashrafian, A., Andersson, H., Manhart, M., 2004. DNS of turbulent flow in
594 rod-roughened channel. *Int. J. Heat and Fluid Flow* 25, 373–383.

595 Bady, M., Kato, S., Huang, H., 2008. Towards the application of indoor
596 ventilation efficiency indices to evaluate the air quality of urban areas.
597 *Build. Environ.* 43, 1991–2004.

598 Baklanov, A., 2009. Introduction to the problem and aims. In: Baklanov,
599 A., Grimmond, S., Mahura, A., Athanassiadou, M. (Eds.), *Meteorological
600 and Air Quality Models for Urban Areas*. Springer, Berlin Heidelberg.

601 Barlow, J. F., Belcher, S. E., 2002. A wind tunnel model for quantifying fluxes
602 in the urban boundary layer. *Boundary-Layer Meteorol.* 104, 131–150.

603 Bentham, T., Britter, R. E., 2003. Spatially averaged flow within obstacle
604 arrays. *Atmos. Environ.* 37, 2037–2043.

605 Britter, R. E., Di Sabatino, S., Caton, F., Cooke, K. M., Simmonds, P. G.,
606 Nickless, G., 2002. Results from three field tracer experiments on the neigh-

- 607 bourhood scale in the city of Birmingham UK. *Water, Air, and Soil Pol-*
608 *lution: Focus 2*, 79–90.
- 609 Brown, M. J., Lawson, R. E., Decroix, D. S., Lee, R. L., 2000. Mean flow and
610 turbulence measurements around a 2-D array of buildings in a wind tunnel.
611 In: *Proceedings of the 11th joint AMS/AWMA Conference in Applied Air*
612 *Pollution Meteorology*, January 2005. Long Beach, CA, USA.
- 613 Cai, X. M., Barlow, J. F., Belcher, S. E., 2008. Dispersion and transfer
614 of passive scalars in and above street canyons - large-eddy simulations.
615 *Atmos. Environ.* 42, 5885–5895.
- 616 Chang, C.-H., Meroney, R. N., 2001. Numerical and physical mod-
617 eling of bluff body flow and dispersion in urban street canyons.
618 *J. Wind Engg. & Ind. Aerodyn.* 89, 1325–1334.
- 619 Chang, C.-H., Meroney, R. N., 2003. Concentration and flow distribu-
620 tions in urban street canyons: wind tunnel and computational data.
621 *J. Wind Engg. & Ind. Aerodyn.* 91, 1141–1154.
- 622 Chang, D., Song, Y., Liu, B., 2009. Visibility trends in six megacities in china
623 1973-2007. *Atmospheric Research* 94, 161–167.
- 624 Chen, J., Wang, W., Zhang, J., Liu, H., Ren, L., Liu, X., Zhang, W., Wang,
625 X., 2009. Characteristics of gaseous pollutants near a main traffic line in
626 beijing and its influencing factors. *Atmospheric Research* 94, 470–480.
- 627 Cheng, W. C., Liu, C.-H., 2011. Large-eddy simulation of flow and pol-
628 lutant transport in and above two-dimensional idealized street canyons.
629 *Boundary-Layer Meteorol.* 139, 411–437.

- 630 Coceal, O., Thomas, T. G., Castro, I. P., Belcher, S. E., 2006. Mean flow and
631 turbulence statistics over groups of urban-like cubical obstacles. *Boundary-*
632 *Layer Meteorol.* 121, 491–519.
- 633 Cui, Z. Q., Cai, X. M., Baker, C. J., 2004. Large-eddy simulation of turbulent
634 flow in a street canyon. *Q. J. R. Meteorol. Soc.* 130, 1373–1394.
- 635 Davidson, M. J., Mylne, K. R., Jones, C. D., Philips, J. C., Perkins, R. J.,
636 Fung, J. C. H., Hunt, J. C. R., 1995. Plume dispersion through large groups
637 of obstacles - a field investigation. *Atmos. Environ.* 29, 3245–3256.
- 638 Douglas, J., Gasiorek, J., Swaffield, J., 1995. *Fluid Mechanics*, 3rd Edition.
639 Longman Scientific & Technical, Essex, UK.
- 640 Hanna, S. R., Brown, M. J., Camelli, F. E., Chan, S. T., Coirier, W. J.,
641 Hansen, O. R., Huber, A. H., Kim, S., Reynolds, R. M., 2006. Detailed
642 simulations of atmospheric flow and dispersion in downtown Manhattan
643 - an application of five computational fluid dynamics models. *BAMS* 87,
644 1713–1726.
- 645 Jiang, Y., Liu, H., Sang, J., Zhang, B., 2007. Numerical and experimental
646 studies on flow and pollutant dispersion in urban street canyons. *Adv. At-*
647 *mos. Sci.* 24, 111–125.
- 648 Kanda, M., 2006. Large-eddy simulations on the effects of surface geome-
649 try of building arrays on turbulent organized structures. *Boundary-Layer*
650 *Meteorol.* 118, 151–168.
- 651 Kastner-Klein, P., Plate, E. J., 1999. Wind-tunnel study of concentration
652 fields in street canyons. *Atmos. Environ.* 33, 3973–3979.

- 653 Kim, J., Moin, P., Moser, R., 1987. Turbulence statistics in fully developed
654 channel flow at low Reynolds number. *J. Fluid Mech.* 177, 133–166.
- 655 Kim Oanh, N. T., Martel, M., Pongkiatkul, P., Berkowicz, R., 2008. Deter-
656 mination of fleet hourly emission and on-road vehicle emission factor using
657 integrated monitoring and modeling approach. *Atmospheric Research* 89,
658 223–232.
- 659 Landsberg, H. E., 1970. Man-made climatic changes. *Energy* 170, 1265–1274.
- 660 Lee, I. Y., Park, H. M., 1994. Parameterization of the pollutant transport
661 and dispersion in urban street canyons. *Atmos. Environ.* 28, 2343–2349.
- 662 Letzel, M. O., Krane, M., Raasch, S., 2008. High resolution urban large-eddy
663 simulation studies from street canyon to neighbourhood scale. *Atmos. En-
664 viron.* 42, 8770–8784.
- 665 Li, X.-X., Liu, C.-H., Leung, D. Y. C., Lam, K. M., 2006. Recent progress
666 in CFD modeling of wind field and pollutant transport in street canyons.
667 *Atmos. Environ.* 40, 5640–5658.
- 668 Liu, C.-H., Barth, M. C., 2002. Large-eddy simulation of flow and scalar
669 transport in a modeled street canyon. *J. Applied Meteor.* 41, 660–673.
- 670 Liu, C.-H., Leung, D. Y. C., Barth, M. C., 2005. On the prediction of air and
671 pollutant exchange rates in street canyons of different aspect ratio using
672 large-eddy simulation. *Atmos. Environ.* 39, 1567–1574.
- 673 Louka, P., Belcher, S. E., Harrison, R. G., 2000. Coupling between air flow in

- 674 streets and the well-developed boundary layer aloft. *Atmos. Environ.* 34,
675 2613–2621.
- 676 Macdonald, R. W., Griffiths, R. F., Hall, D. J., 1998. A comparison of results
677 from scaled field and wind tunnel modelling of dispersion in arrays of
678 obstacles. *Atmos. Environ.* 32, 3845–3862.
- 679 Mazzeo, N. A., Venegas, L. E., 1991. Air pollution model for an urban area.
680 *Atmospheric Research* 26, 165–179.
- 681 Meroney, R. A., Pavageau, M., Rafailidis, S., Schatzmann, M., 1996. Study
682 of line source characteristics for 2-D physical modelling of pollutant dis-
683 persion in street canyons. *J. Wind Engg. & Ind. Aerodyn.* 90, 321–339.
- 684 Michioka, T., Sato, A., 2012. Effect of incoming turbulent structure on pol-
685 lutant removal from two-dimensional street canyon. *Boundary Layer Me-
686 teorol.* 145, 469–484.
- 687 Michioka, T., Sato, A., Sada, K., 2011a. Wind-tunnel experiments for gas
688 dispersion in an atmospheric boundary layer with large-scale turbulent
689 motion. *Boundary Layer Meteorol.* 141, 35–51.
- 690 Michioka, T., Sato, A., Takimoto, H., Kanda, M., 2011b. Large-eddy simula-
691 tion for the mechanism of pollutant removal from a two-dimensional street
692 canyon. *Boundary Layer Meteorol.* 138, 195–213.
- 693 Minoura, H., 1999. Some characteristics of surface ozone concentration ob-
694 served in an urban atmosphere. *Atmospheric Research* 51, 153–169.

- 695 Nagaosa, R., 1999. Direct numerical simulation of vortex structures and tur-
696 bulent shear transfer across a free surface in a fully developed turbulence.
697 Phys. Fluids 11, 1581–1595.
- 698 Narita, K., 2007. Experimental study of the transfer velocity for urban sur-
699 faces with a water evaporation method. Boundary-Layer Meteorol. 122,
700 293–320.
- 701 Notario, A., Bravo, I., Adame, J. A., Díaz-de Mera, Y., Aranda, A.,
702 Rodríguez, A., Rodríguez, D., 2012. Analysis of NO, NO₂, NO_x, O₃ and
703 oxidant (OX = O₃ + NO₂) levels measured in a metropolitan area in the
704 southwest of iberian Peninsula. Atmospheric Research 104-105, 217–226.
- 705 Oke, T. R., 1988. Street design and urban canopy layer climate. Energy Bldg.
706 11, 103–113.
- 707 OpenFOAM, 2013. OpenFOAM: The open source CFD toolbox.
708 [Http://www.openfoam.com/](http://www.openfoam.com/).
- 709 Parrish, D. D., Zhu, T., 2009. Clean air for megacities. Science 326, 674–675.
- 710 Pasquill, F., 1983. Atmospheric Diffusion. John Wiley & Sons, New York,
711 USA.
- 712 Pavageau, M., Schatzmann, M., 1999. Wind tunnel measurements of con-
713 centration fluctuations in an urban street canyon. Atmos. Environ. 33,
714 3961–3971.
- 715 Piringer, M., Joffre, S., Baklanov, A., Christen, A., Deserti, M., De Ridder,
716 K., Emeis, S., Mestayer, P. amd Tombrou, M., Middleton, D., Baumann-

- 717 Stanzer, K., Dandou, A., Karppinen, A., Burzynski, J., 2007. The surface
718 energy balance and the mixing height in urban areas - activities and rec-
719 ommendations of COST-Action 715. *Boundary-Layer Meteorol.* 124, 2–24.
- 720 Pope, S. B., 2009. *Turbulent flow*, sixth Edition. Cambridge University Press,
721 Cambridge, UK.
- 722 Rotach, M. W., Vogt, R., Bernhofer, C., Batchvarova, E., Christen, A., Clap-
723 pier, A., Feddersen, B., Gryning, S.-E., Martucci, G., Mayer, H., Mitev,
724 V., Oke, T. R., Parlow, E., Richner, H., Roth, M., Roulet, Y.-A., D., R.,
725 Salmond, J. A., Schatzmann, M., Voogt, J. A., 2005. BUBBLE - an urban
726 boundary layer meteorology project. *Theor. Appl. Climatol.* 81, 231–261.
- 727 Roth, M., 2000. Review of atmospheric turbulence over cities. *Q. J. R. Me-*
728 *eteorol. Soc.* 126, 941–990.
- 729 Schumann, U., 1975. Subgrid scale model for finite difference simulations of
730 turbulent flows in plane channels and annuli. *J. Comp. Phys.* 18, 376–404.
- 731 Sini, J. F., Anquetin, S., Mestayer, P. G., 1996. Pollutant dispersion and
732 thermal effects in urban street canyons. *Atmos. Environ.* 30, 2659–2677.
- 733 Smagorinsky, J., 1963. General circulation experiments with the primitive
734 equations I: The basic experiment. *Month. Weath. Rev.* 91, 99–165.
- 735 Spalding, D. B., 1962. A new analytical expression for the drag of a flat
736 plate valid for both the turbulent and laminar regimes. *J. Heat and Mass*
737 *Transfer* 5, 1133–1138.

- 738 Takimoto, H., Sato, A., Barlow, J. F., Moriwaki, R., Inagaki, A., Onomura,
739 S., Kanda, M., 2011. Particle image velocimetry measurements of turbulent
740 flow within outdoor and indoor urban scale models and flushing motions
741 in urban canopy layers. *Boundary-Layer Meteorol.* 140, 295–314.
- 742 Tu, J., Xia, Z.-G., Wang, H., Li, W., 2007. Temporal variations in surface
743 ozone and its precursors and meteorological effects at an urban site in
744 china. *Atmospheric Research* 85, 310–337.
- 745 United Nation, 2008. *World Urbanization Prospects: The 2007 Revision*
746 *Highlight*. United Nation, New York.
- 747 Vardoulakis, S., Fisher, B.-E., Pericleous, K., Gonzalez-Flesca, N., 2003.
748 *Modelling air quality in street canyons: A review*. *Atmos. Environ.* 37,
749 155–182.
- 750 Wong, C. C. C., Liu, C.-H., 2010a. On the pollutant plume dispersion in
751 the urban canopy layer over 2D idealized street canyons: a large-eddy
752 simulation approach. In: *European Geosciences Union General Assembly*
753 *2010, May 2 to 7, 2010. Vienna, Austria*.
- 754 Wong, C. C. C., Liu, C.-H., 2010b. Pollutant removal, dispersion and entrain-
755 ment over two-dimensional idealized street canyons: an LES approach. In:
756 *American Geophysical Union Fall Meeting 2010, December 13 to 17, 2010.*
757 *San Francisco, California, USA*.
- 758 Wood, R. C., Arnold, S. J., Balogun, A. A., Barlow, J. F., Belcher, S. E.,
759 Britter, R. E., Cheng, H., Dobre, A., Lingard, J. J. N., Martin, D., Neo-
760 phytou, M. K., Petersson, F. K., Robins, A. G., Smallcross, D. E., Smalley,

- 761 R. J., Tate, J. E., Tomlin, A. S., White, I. R., 2009. Dispersion experiments
762 in central London. *Q. J. R. Meteorol. Soc.* 90, 955–969.
- 763 Yee, E., Gailis, R. M., Hill, A., Hilderman, T., Kiel, D., 2006. Comparison
764 of wind-tunnel and water-channel simulations of plume dispersion through
765 a large array of obstacles with a scaled field experiment. *Boundary-Layer*
766 *Meteorol.* 121, 389–432.

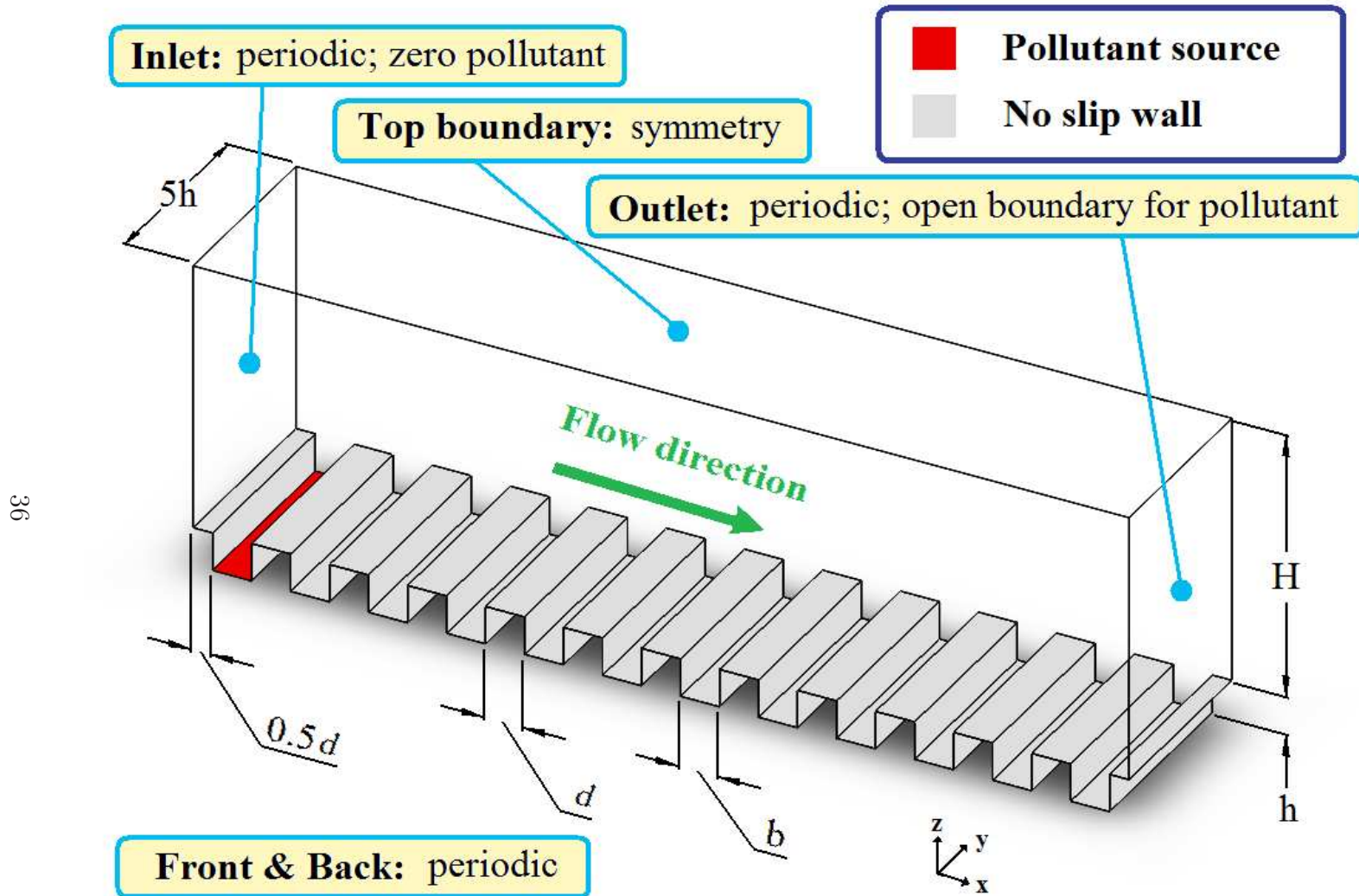


Figure 1: Computational domain of the LES. Note that $d = b = h$ in the current study.

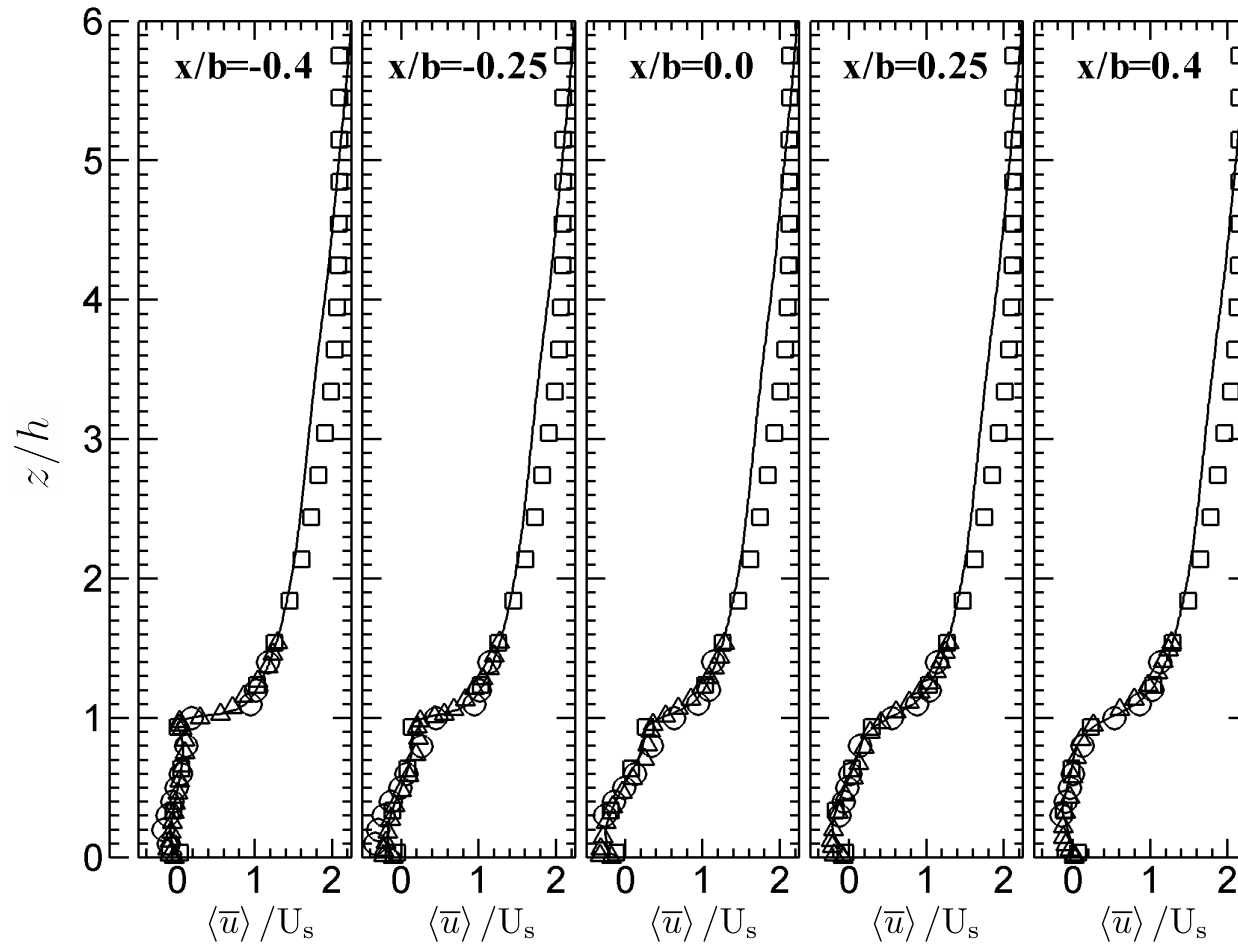


Figure 2: Vertical profiles of the ensemble average streamwise velocity $\langle \bar{u} \rangle / U_s$. \circ : Brown et al. (2000); Δ : Cui et al. (2004); \square : LES of Cheng and Liu (2011); and $—$: current LES;

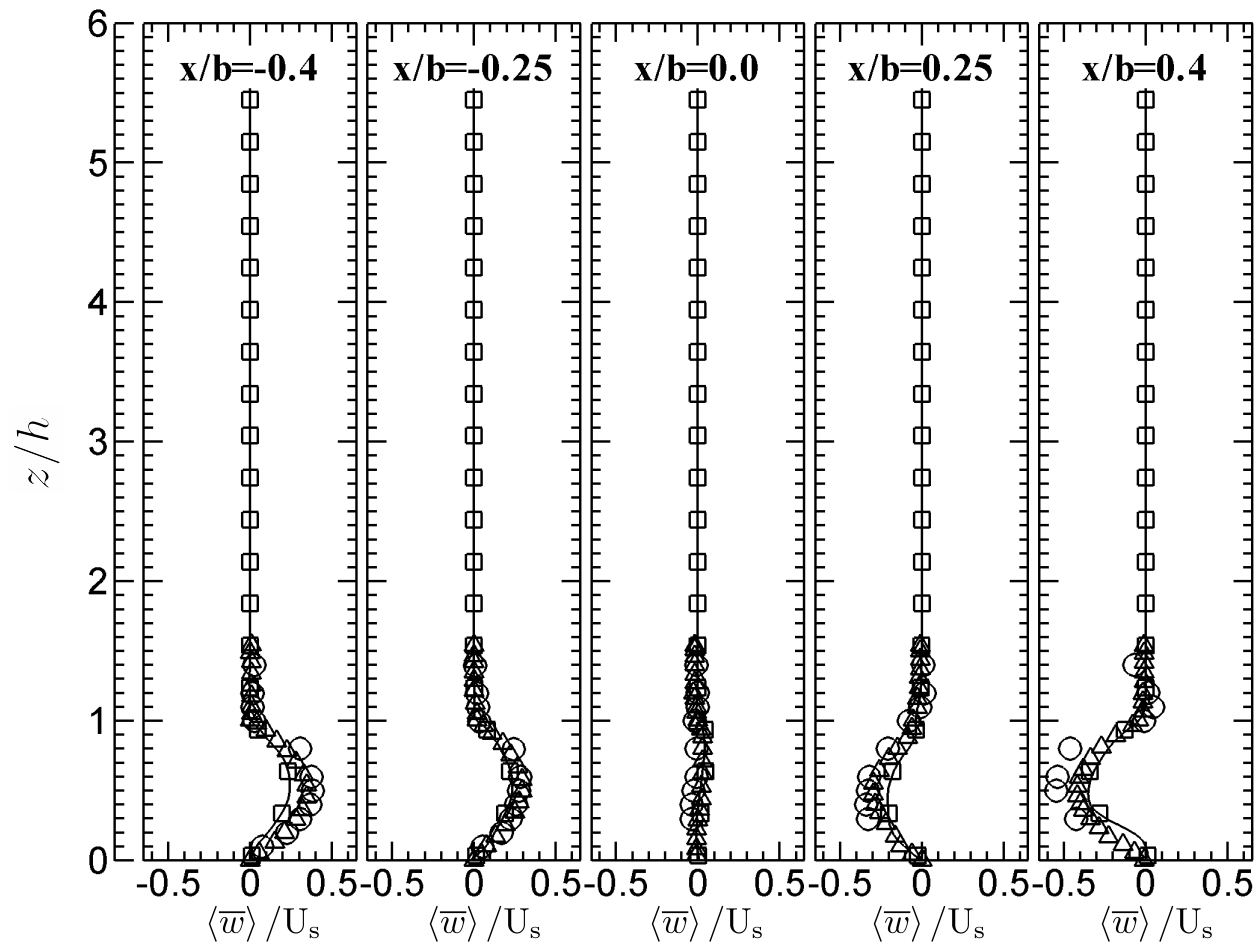


Figure 3: Vertical profiles of the ensemble average vertical velocity $\langle \bar{w} \rangle / U_s$. \circ : Brown et al. (2000); Δ : Cui et al. (2004); \square : LES of Cheng and Liu (2011); and $—$: current LES;

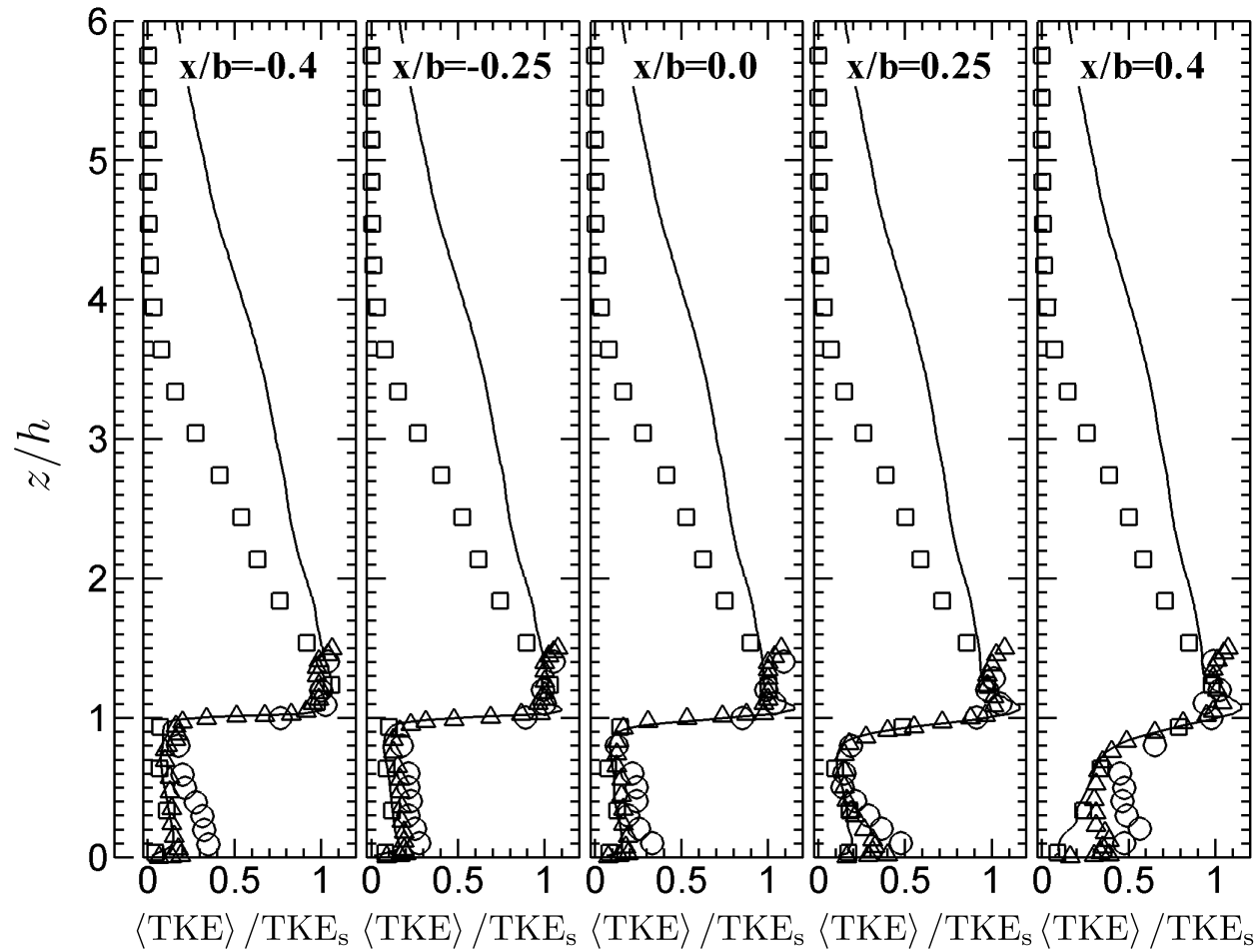


Figure 4: Vertical profiles of the ensemble average turbulent kinetic energy $\langle \text{TKE} \rangle / \text{TKE}_s$. \circ : Brown et al. (2000); Δ : Cui et al. (2004); \square : LES of Cheng and Liu (2011); and —: current LES;

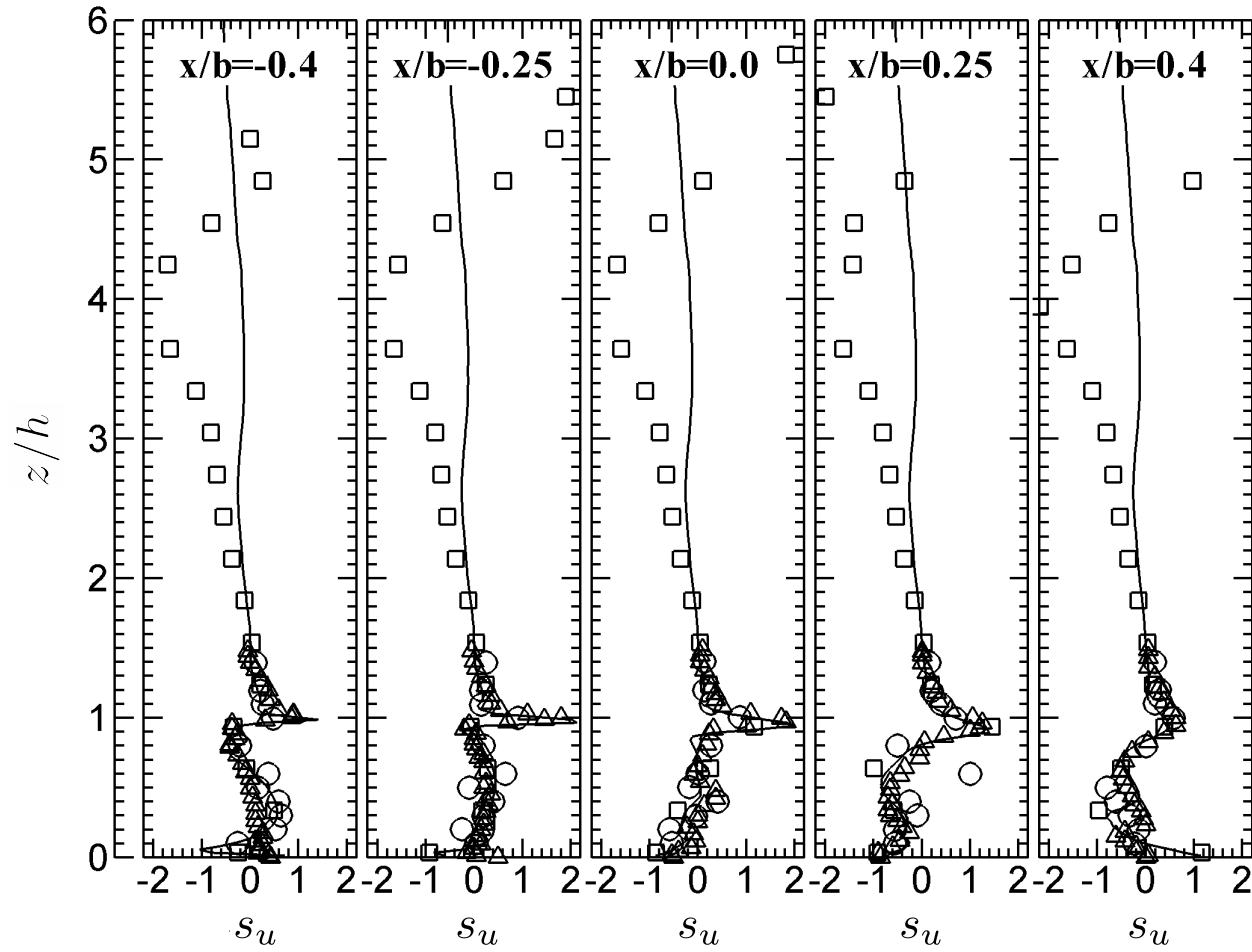


Figure 5: Vertical profiles of the skewness of the streamwise velocity s_u . \circ : Brown et al. (2000); Δ : Cui et al. (2004); \square : LES of Cheng and Liu (2011); and $—$: current LES;

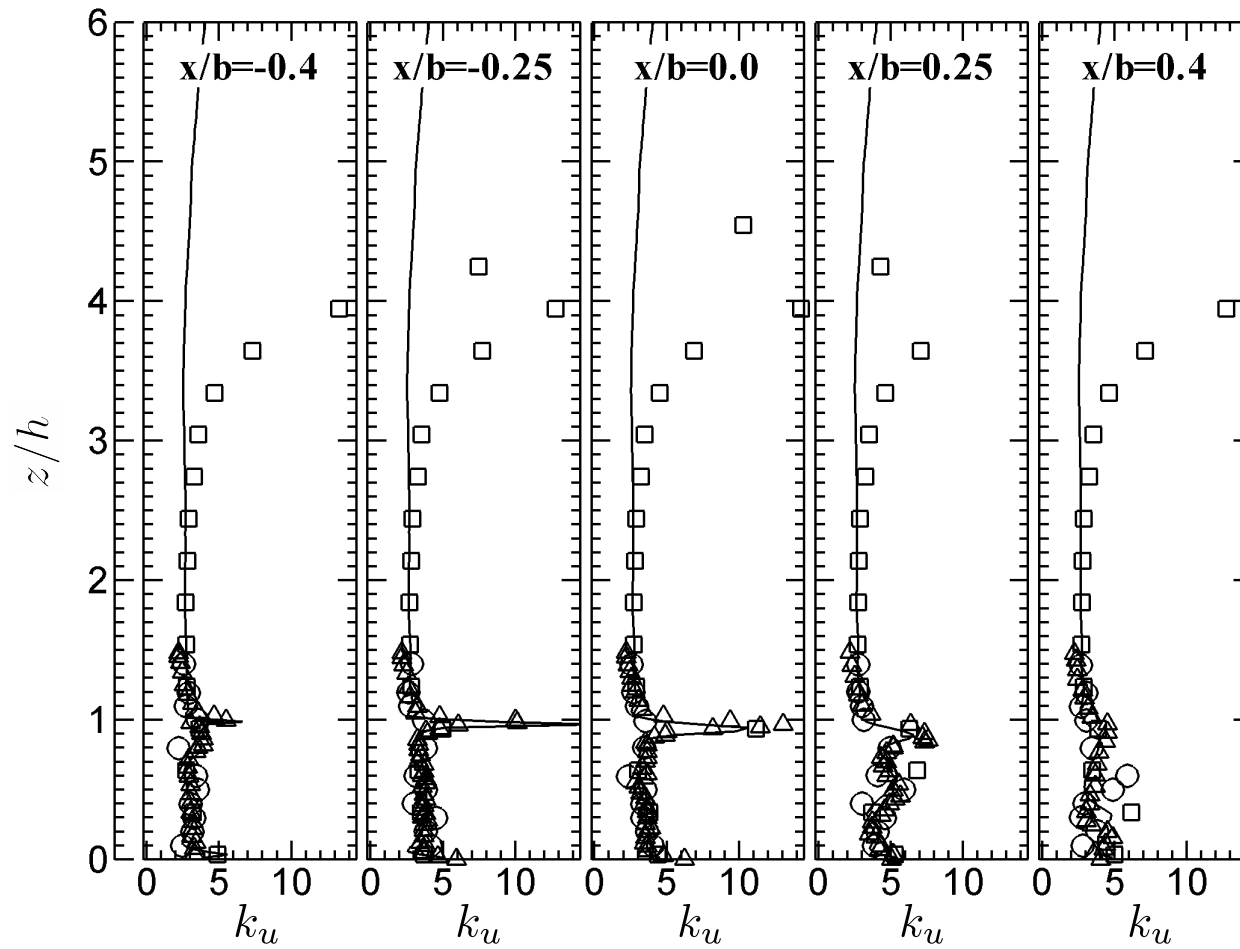


Figure 6: Vertical profiles of the kurtosis of the streamwise velocity k_u . \circ : Brown et al. (2000); Δ : Cui et al. (2004); \square : LES of Cheng and Liu (2011); and $—$: current LES;

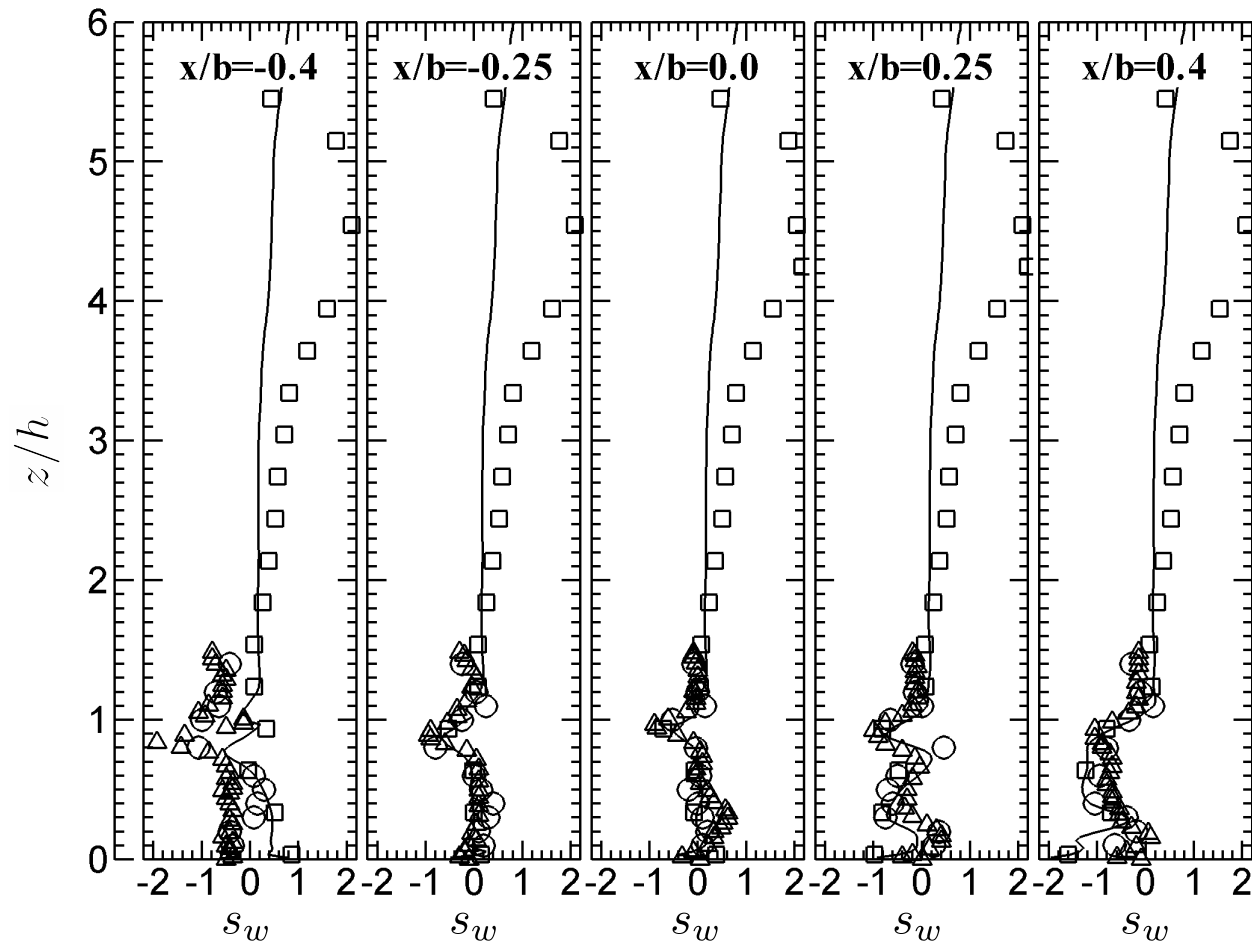


Figure 7: Vertical profiles of the skewness of the vertical velocity s_w . \circ : Brown et al. (2000); Δ : Cui et al. (2004); \square : LES of Cheng and Liu (2011); and $—$: current LES;

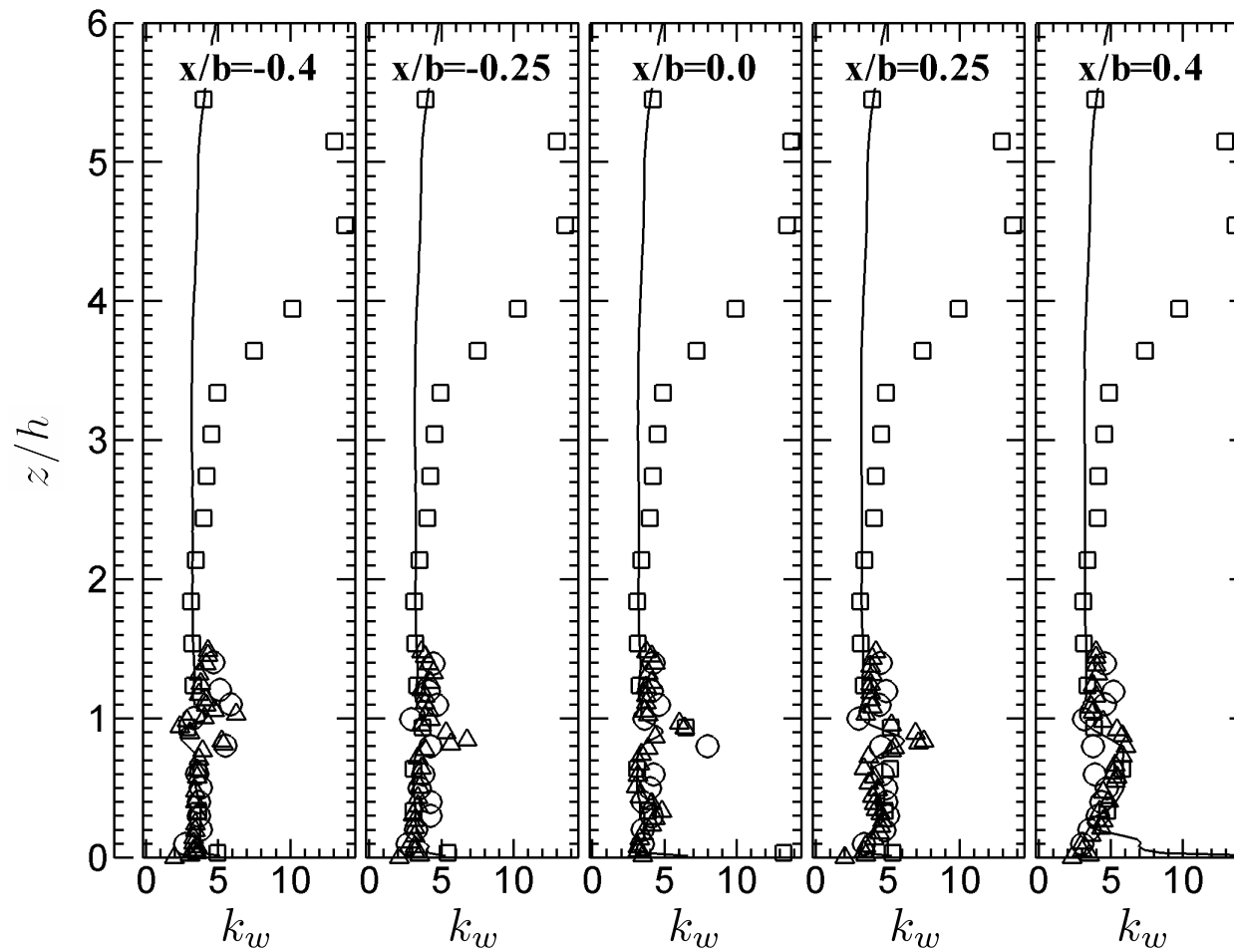


Figure 8: Vertical profiles of the kurtosis of the vertical velocity k_w . \circ : Brown et al. (2000); Δ : Cui et al. (2004); \square : LES of Cheng and Liu (2011); and $—$: current LES;

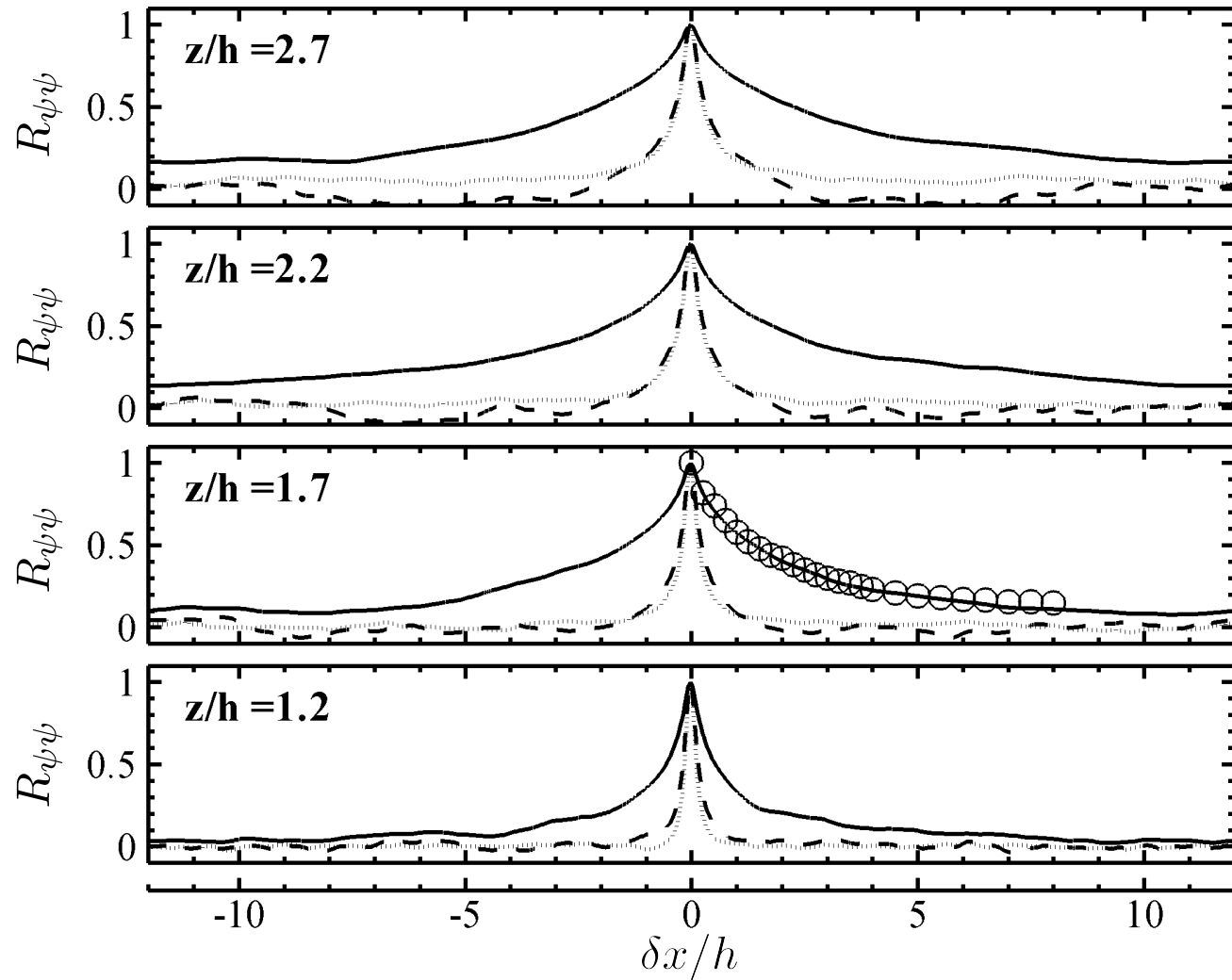


Figure 9: Autocorrelation $R_{\psi\psi}(x_0 = 0, \delta x)$ in the streamwise direction x . —: R_{uu} ; - - - - -: R_{vv} ; and $\cdots\cdots$: R_{ww} of current LES. Also shown is R_{uu} over an array of cubes. \circ : Coccal et al. (2006).

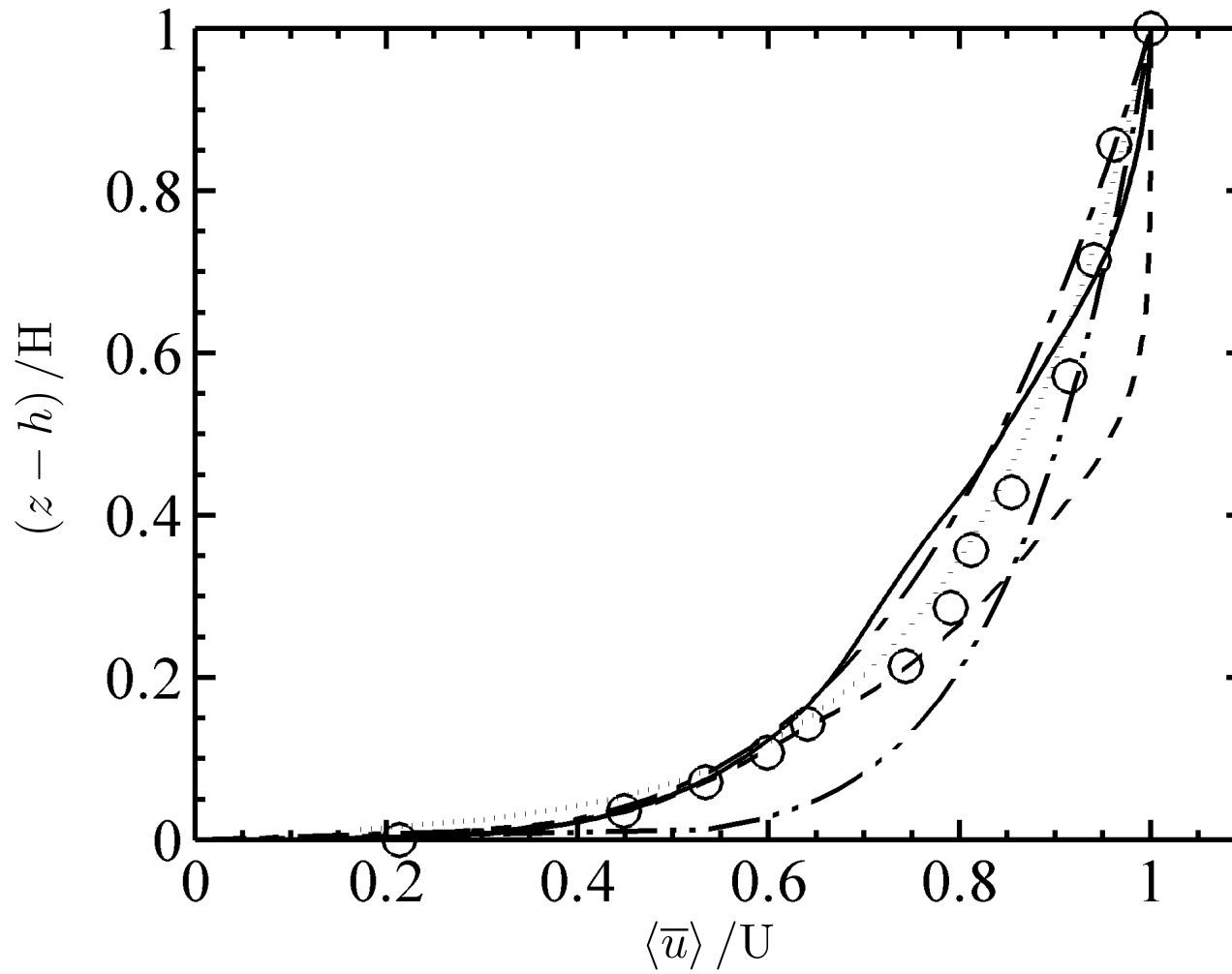


Figure 10: Vertical profiles of dimensionless streamwise velocity $\langle \bar{u} \rangle / U$. —: current LES; - - - - -: Cheng and Liu (2011); \circ : Coceal et al. (2006); - · - · - : 1/4 power law; - · - - · - : 1/7 power law; and ······: log law.

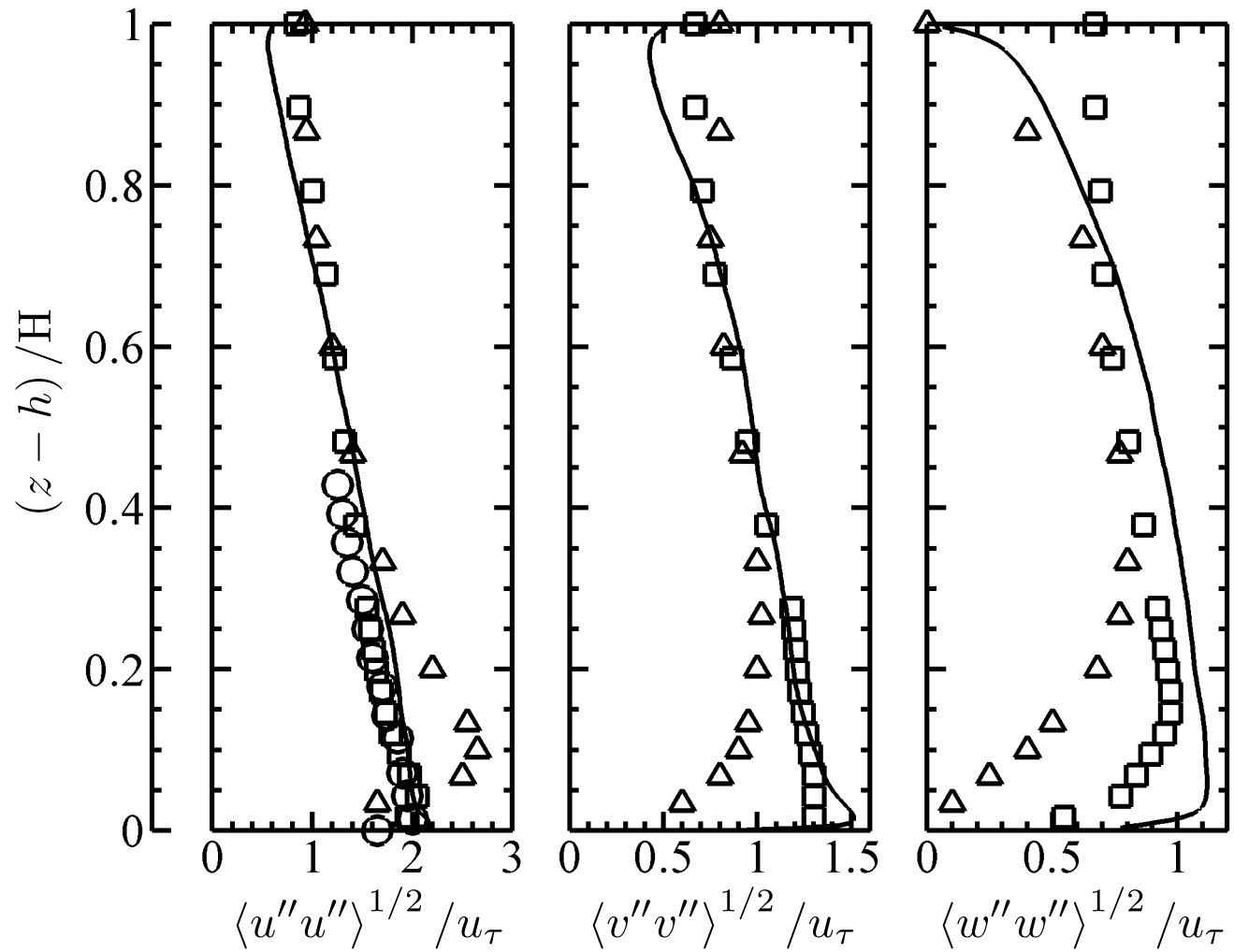


Figure 11: Vertical profiles of dimensionless root-mean-square velocity fluctuation $\langle u''u'' \rangle^{1/2} / u_\tau$. —: current LES; Δ : Nagaosa (1999); \square : Ashrafian et al. (2004); and \circ : Coceal et al. (2006).

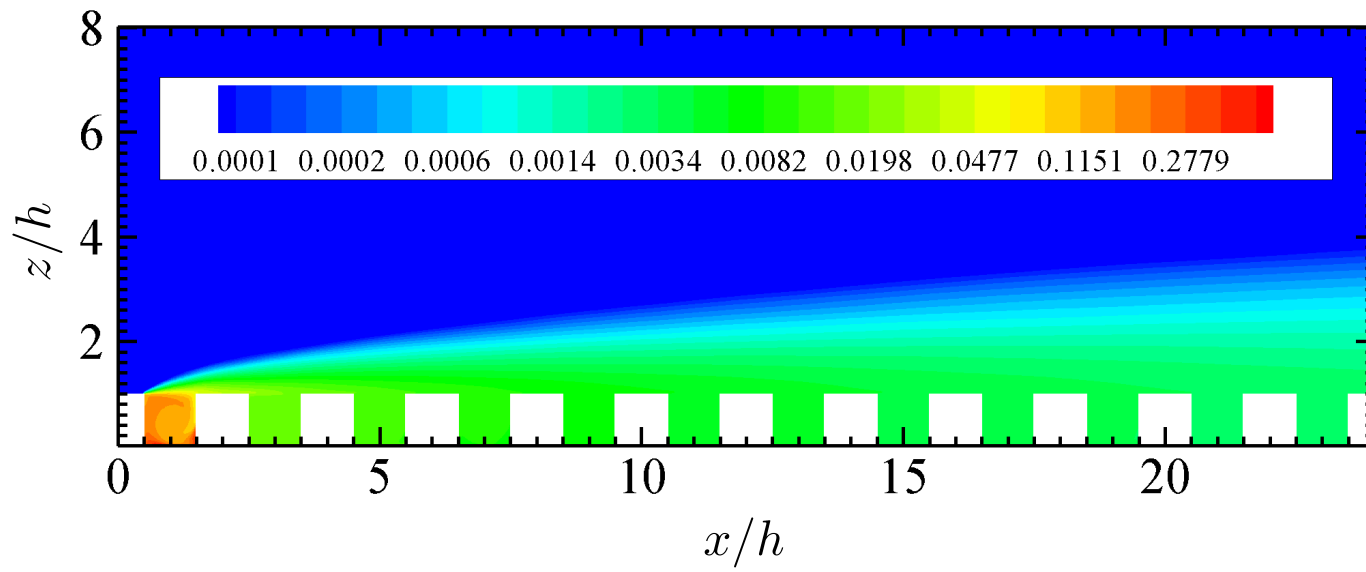


Figure 12: Contours of ensemble average pollutant concentration $\langle \bar{\phi} \rangle / \Phi$ on the vertical x - z plane.

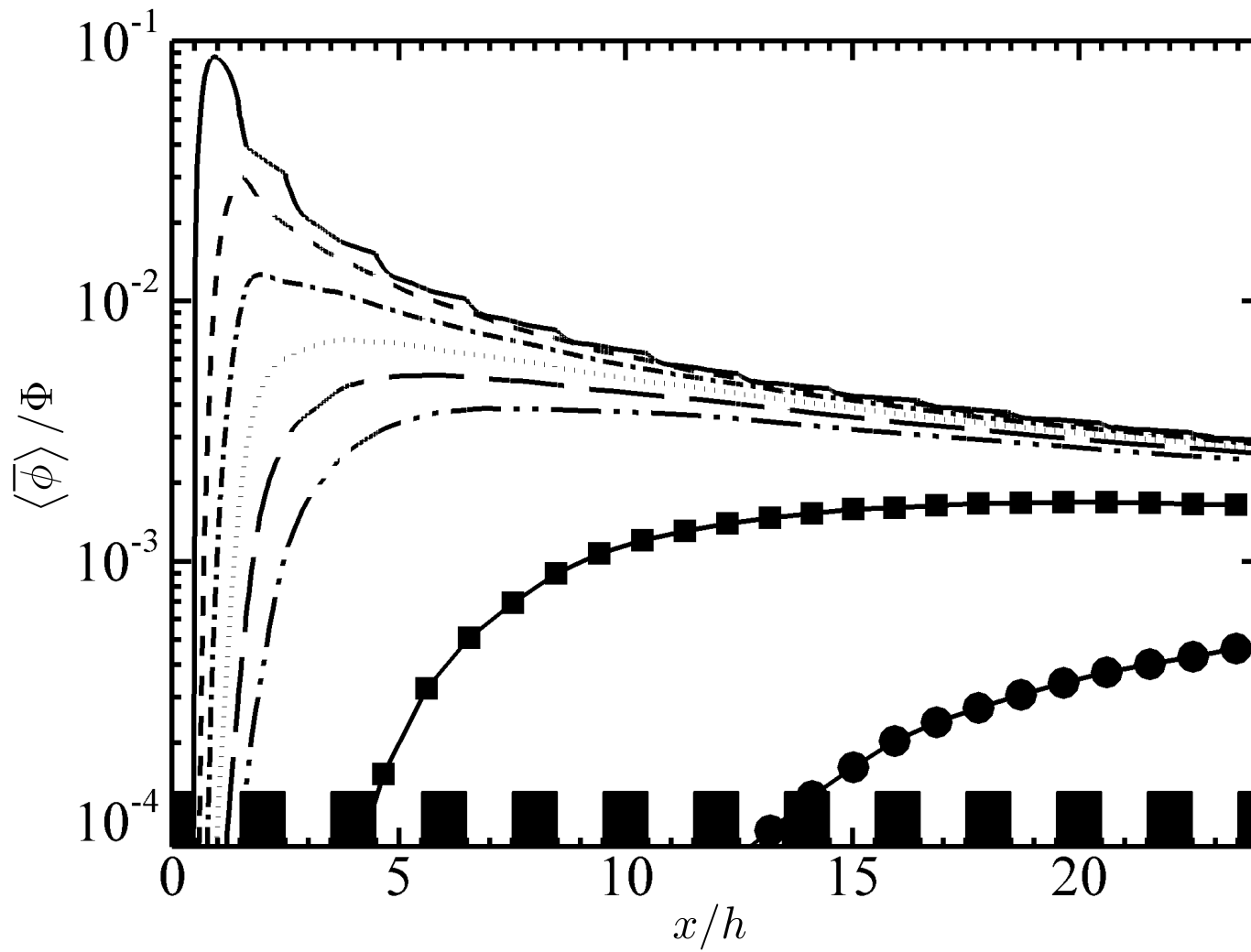


Figure 13: Ensemble average pollutant concentration $\langle \bar{\phi} \rangle / \Phi$ plotted as a function of streamwise distance x/h at different elevations $z = :$ —: h ; - - - - -: $1.1h$; - · - · -: $1.2h$; ·····: $1.3h$; — — — — —: $1.4h$; - · - · - · -: $1.5h$; — ■ — ■ —: $2h$; and — ● — ● —: $3h$.

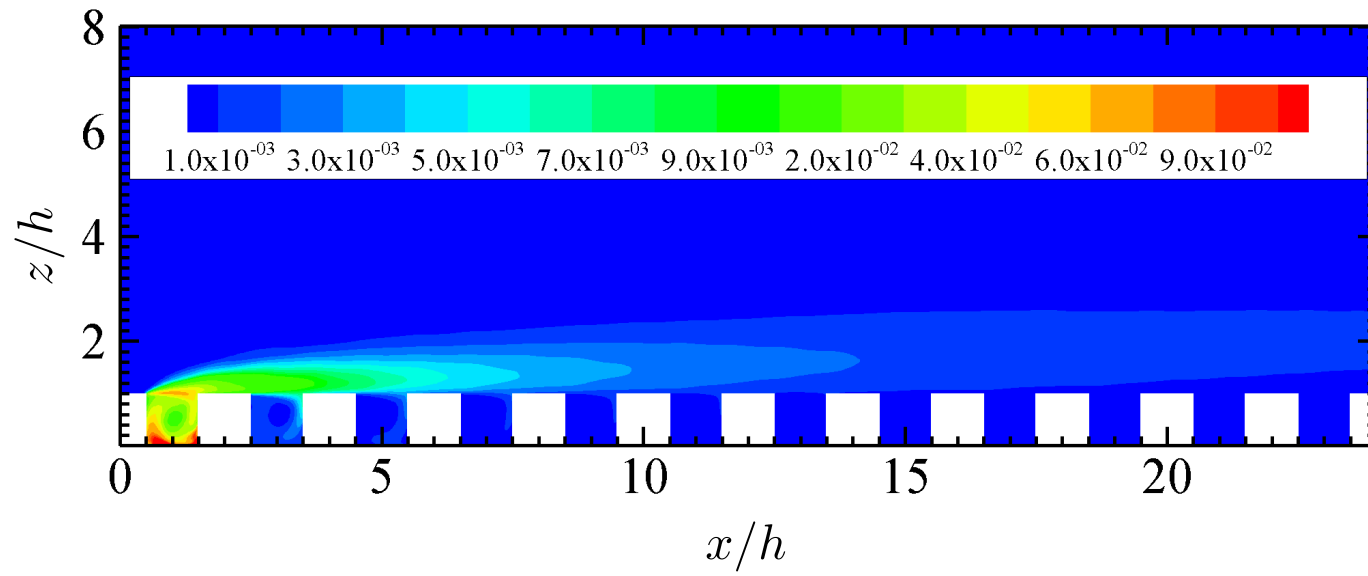


Figure 14: Contours of root-mean-square pollutant concentration $\langle \phi'' \phi'' \rangle^{1/2} / \Phi$ on the vertical x - z plane.

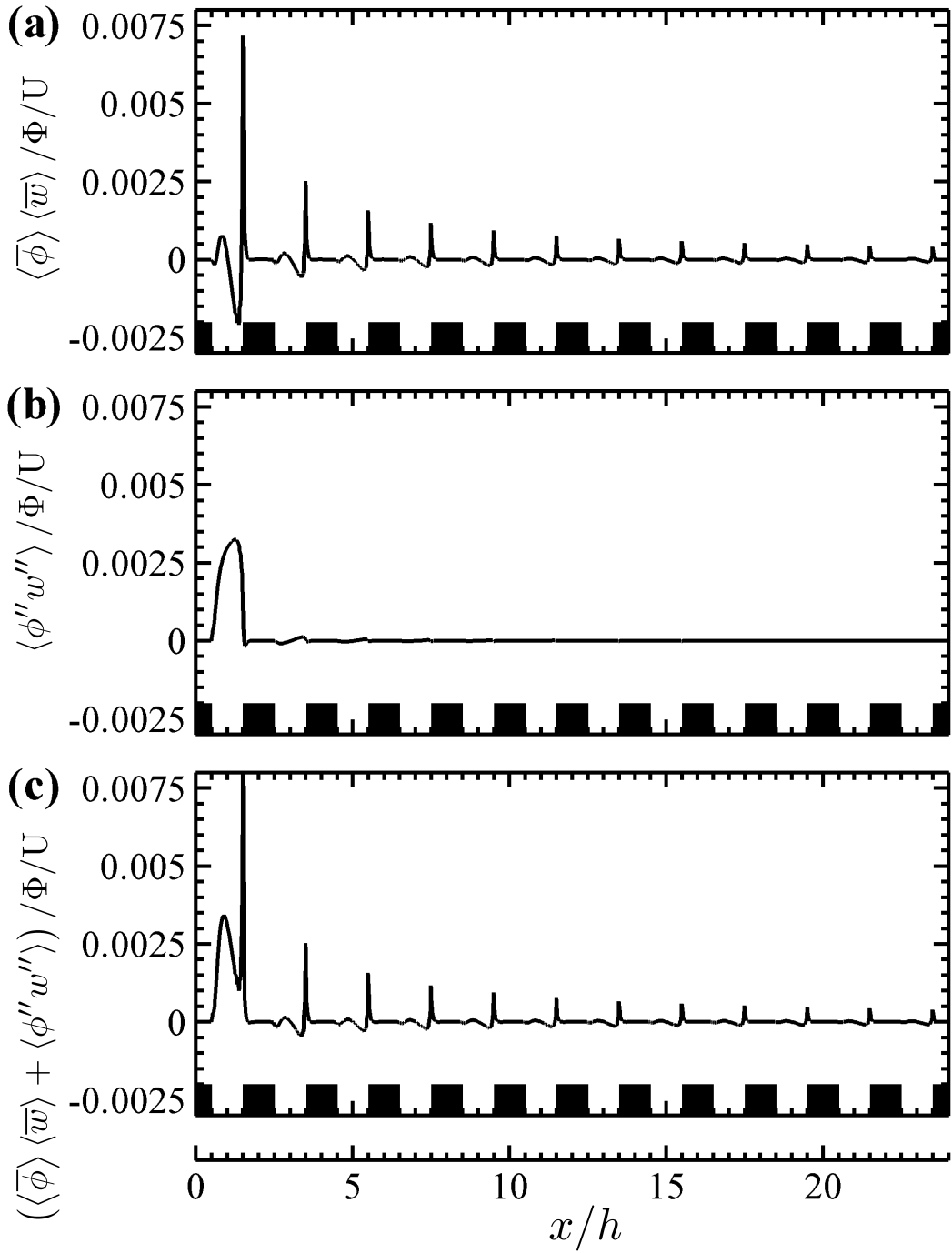


Figure 15: Ensemble average vertical pollutant flux along the roof level.

- (a). Mean component $\langle \bar{\phi} \rangle \langle \bar{w} \rangle / \Phi / U$; (b). turbulent component $\langle \phi'' w'' \rangle / \Phi / U$; and (c). total vertical pollutant flux $(\langle \bar{\phi} \rangle \langle \bar{w} \rangle + \langle \phi'' w'' \rangle) / \Phi / U$.

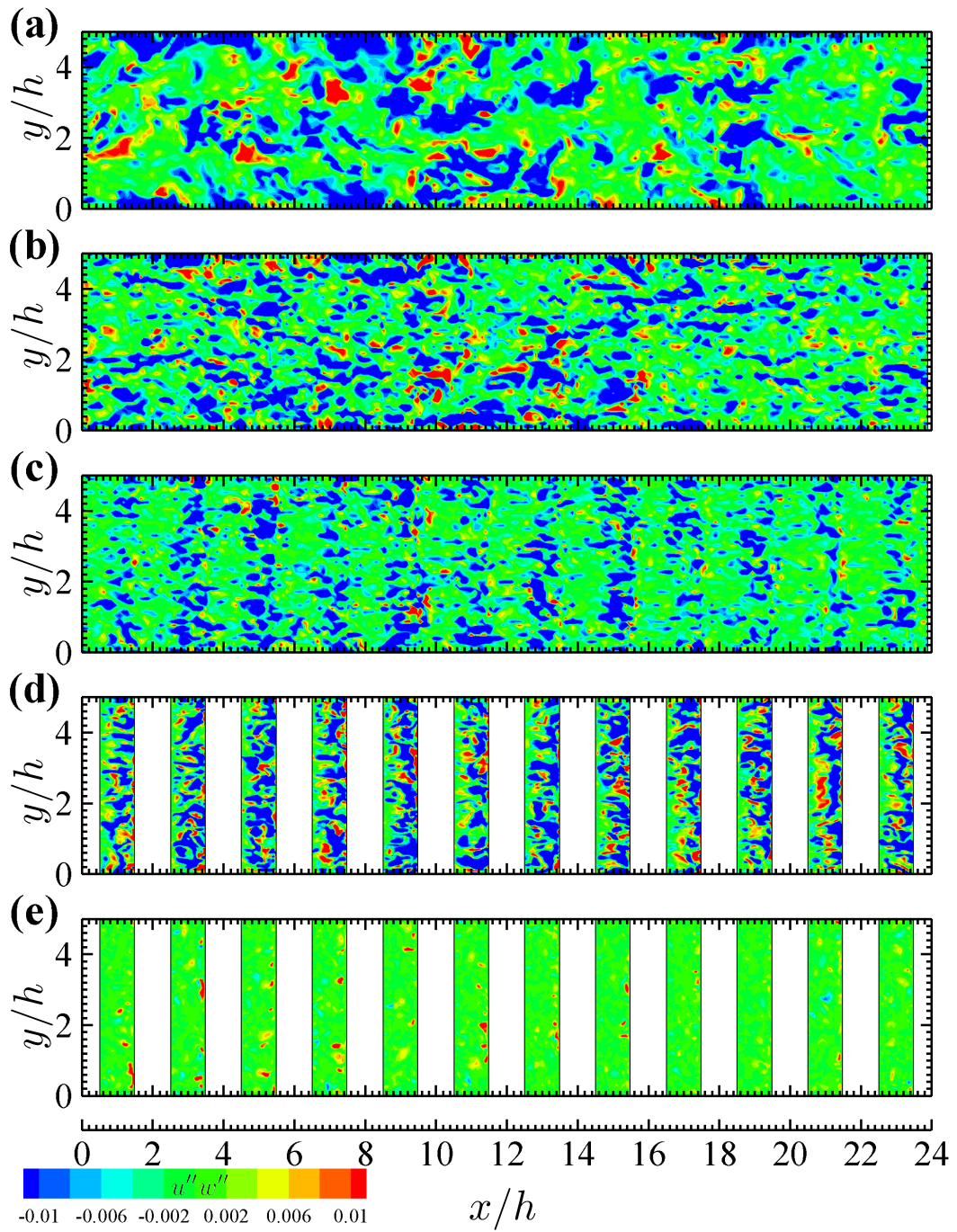


Figure 16: Contours of vertical momentum flux $u''w''/U^2$ on the horizontal planes at $z =$ (a). $2h$; (b). $1.2h$; (c). $1.05h$; (d). h ; and (e). $0.5h$.

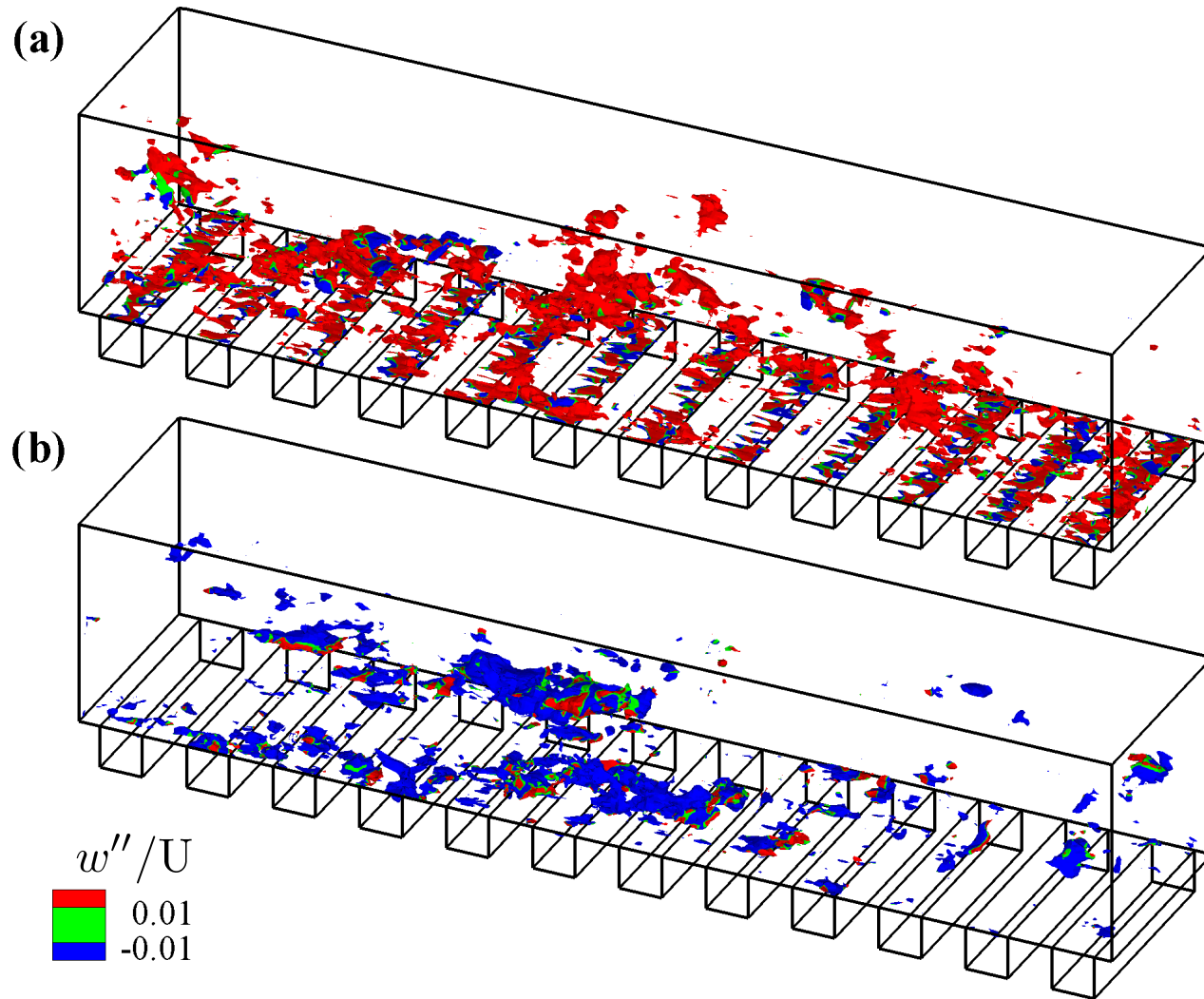


Figure 17: Isosurface of streamwise fluctuating velocity $u'' =$: (a). $-0.25U$ and (b). $0.25U$. Also shown are the contours of vertical fluctuating velocity w''/U .

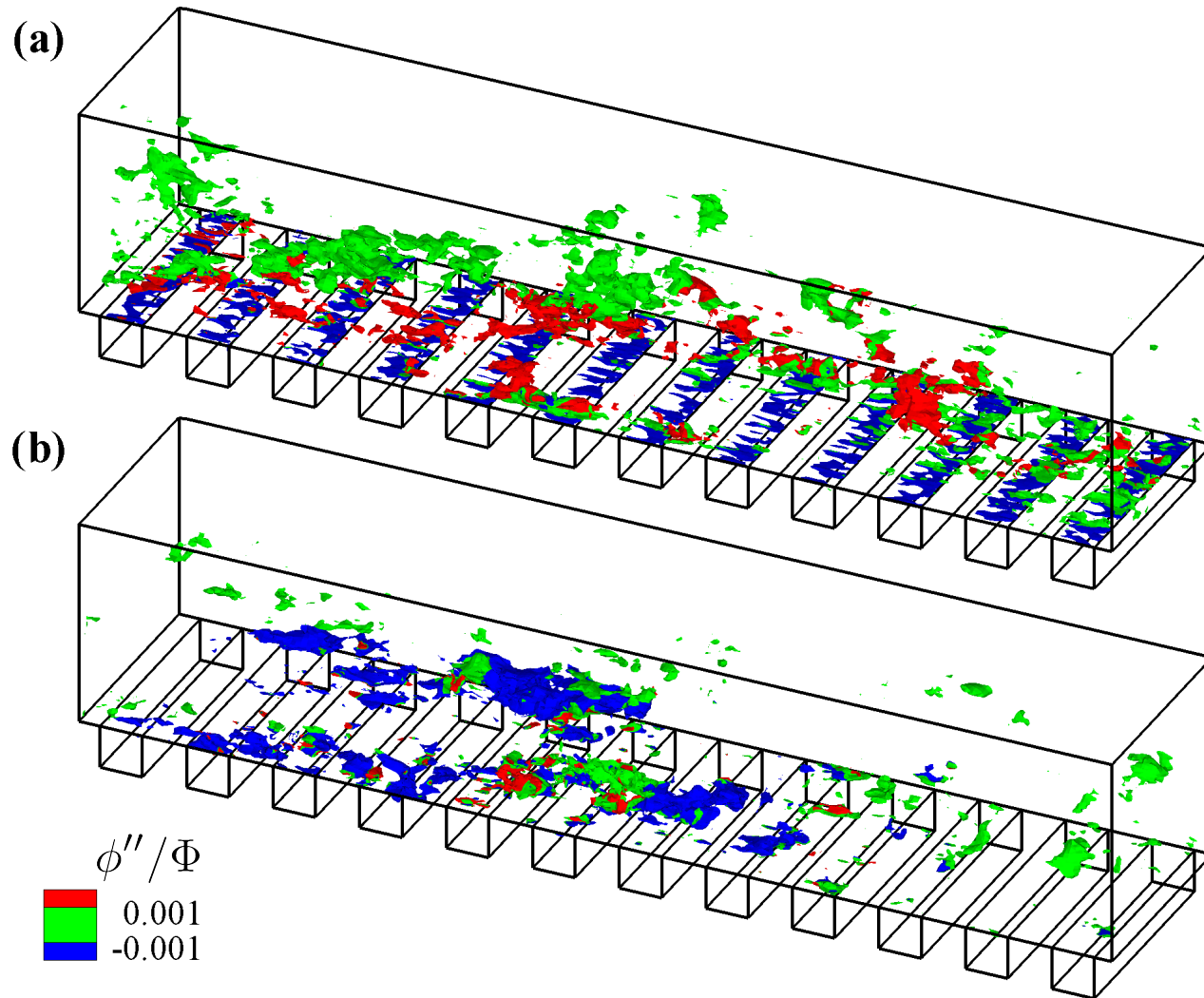


Figure 18: Isosurface of streamwise fluctuating velocity $u'' =$: (a). $-0.25U$ and (b). $0.25U$. Also shown are the contours of fluctuating pollutant concentration ϕ''/Φ .

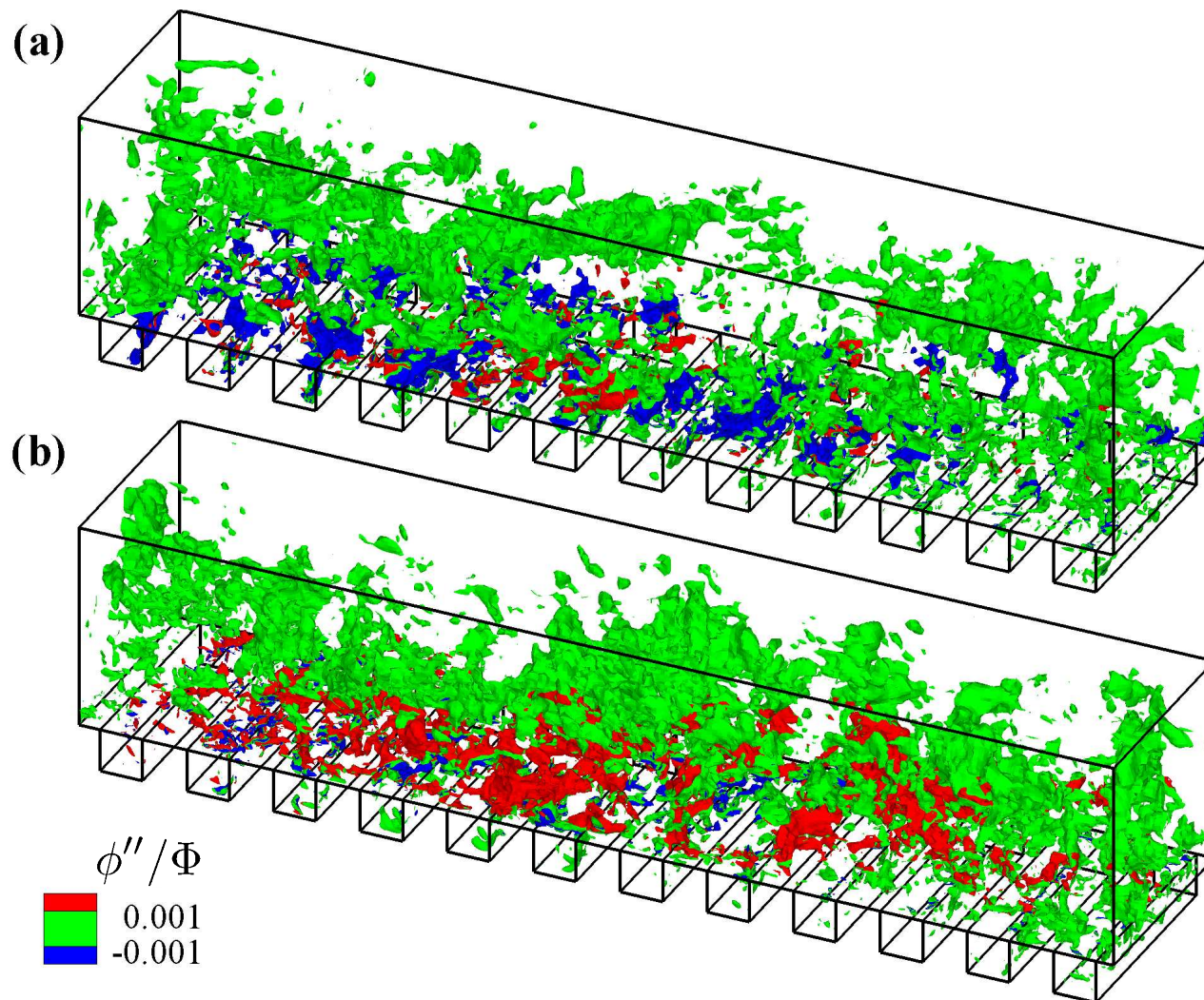


Figure 19: Isosurface of vertical fluctuating velocity $w'' =$: (a). $-0.1U$ and (b). $0.1U$. Also shown are the contours of fluctuating pollutant concentration ϕ''/Φ .